DISPLACIVE WIDENING OF CALCITE VEINS IN SHALE: INSIGHTS INTO FORCE OF CRYSTALLIZATION

QINGFENG MENG, JOHN HOOKER, AND JOE CARTWRIGHT

Department of Earth Sciences, University of Oxford, South Parks Road, Oxford, OX1 3AN, UK

e-mail: meng.qingfeng@hotmail.com

ABSTRACT: The geometry, microtextures, and *c*-axis fabrics of calcite "beef" veins in the Lower Jurassic black shales (Wessex Basin, UK) were characterized to investigate the mechanism responsible for widening following fracture propagation. Isolated beef veins exhibit planar tapering tips, whereas closely spaced veins are characterized by blunt tips. Vein surfaces are generally smooth and flat; however, circular ridges appear on vein surfaces that protrude into the host clays where there are solid inclusions below or above the ridges. Fossils with well-preserved morphologies, which are separated by subvertical calcite fibers, are observed on both the lower and upper surfaces of single veins. The shale laminations around beef veins are folded and parallel to vein margins. The beef veins commonly contain blocky zones of small, equant calcite crystals, pyrite, and organic matter. The fibers exhibit a preferred subvertical *c*-axis orientation, whilst crystals in the median zones and blocky zones have random *c*-axis orientations. The different crystal sizes, morphologies, and *c*-axis orientations of the fibers from the blocky crystals suggest that the fibers grew without competition with each other under a nonhydrostatic stress field. The displacive widening of calcite beef veins, which is evident from vein interactions and deformation of individual fossil skeletons, demonstrates that fibers grew

incrementally because the crystallization pressure of calcite exceeded the overburden load. The force of crystallization is suggested to be responsible for the *c*-axis orientations of calcite fibers, whereby crystals with free surfaces normal to *c*-axis orientations grew preferentially. The present study suggests that the fibrous widening of calcite veins in shale postdates their initiation and may result from displacive crystallization rather than fluid overpressure.

Keywords: displacive; shale; fibrous; force of crystallization; *c*-axis

INTRODUCTION

Fibrous calcite veins, also known as "beef", consist of fibrous calcite crystals and lie parallel to bedding (Selles-Martinez, 1996; Bons et al., 2012; Cobbold et al., 2013; Gale et al., 2014). Calcite beef veins are common diagenetic structures in shales and less common in thin limestone beds in sedimentary basins worldwide (Cobbold et al., 2013). Beef veins have been studied since the 1860s (Sorby, 1860), and are significant for understanding host-rock diagenesis and deformation, fluid pressure, and composition when the veins formed (e.g., Tarr, 1933; Marshall, 1982; El-Shahat and West, 1983; Urai et al., 1991; Al-Aasm et al., 1995; Kiriakoulakis et al., 2000; Hilgers and Urai, 2005; Parnell et al., 2014; Hooker and Cartwright, 2016; Meng et al., 2017). However, their formation mechanism remains controversial. Ramsay (1980) suggested that fibrous mineral veins owe their origin to crack-seal mechanism, i.e., episodic crack opening by oscillations in fluid pressure. However, recent studies have revealed that the crack-seal mechanism may not be applicable for beef veins that exhibit an antitaxial pattern, where fibrous crystals grow continuously towards the host rock and lack characteristic inclusion bands and trails (Bons, 2000; Means and Li, 2001; Bons and Montenari, 2005). Nevertheless, overpressure

in low-permeability sediments is generally acknowledged to play an important role in vein nucleation (Stoneley, 1983; Rodrigues et al., 2009; Cobbold et al., 2013).

The difficulty in understanding the origin of beef veins lies in the opening mechanism against overburden load whilst simultaneously allowing incremental calcite precipitation (Stoneley, 1983). This process is capable of forming veins with an aperture up to 10 cm (Fisher et al., 1995). Many researchers have attributed this mechanism to overpressure (Al-Aasm et al., 1995; Parnell and Carey, 1995; Selles-Martinez, 1996; Oliver and Bons, 2001; Basson and Viola, 2004). When fluid pressure exceeds the overburden stress, the vertical effective stress becomes tensile and results in horizontal fractures if the fluid pressure is distributed and there are no tectonic stresses (Cobbold and Rodrigues, 2007). Based on the occurrence of oil residues in calcite beef veins in black shales, it has been suggested that primary oil migration could be responsible for overpressure buildup, tensile fracturing, and also holding apart fracture walls during calcite precipitation (e.g., Stoneley, 1983; Parnell et al., 2000; Rodrigues et al., 2009; Cobbold et al., 2013; Zanella et al., 2014a and b, 2015a and b; Hooker at al., 2016). Many other factors controlled by chemical compaction could also result in overpressure in shales during burial, such as mineral diagenesis with dehydration (mainly smectite-to-illite transformation, gypsum-to-anhydrite transforamtion) (e.g., Freed and Peacor, 1989; Jowett et al., 1993; Osborne and Swarbrick, 1997; Lahann and Swarbrick, 2011; Bols et al., 2004) and generation of methane gas (e.g., Hedberg, 1974; Flemings et al., 2003; Lash and Engelder, 2005; Meng et al., 2017).

An alternative explanation for the widening of fibrous veins favors the force of crystallization (Watts, 1978; Means and Li, 2001; Wiltschko and Morse, 2001), which provides the necessary space for fibers to grow incrementally without significant void space being created during the growth episode (Bons and Jessell, 1997). It has been long been known that the growth of crystals

65 can produce a crystallization pressure exerted on its surroundings as a result of mechano-
66 chemical interaction between minerals in the host rock and the solution (Weyl, 1959; Maliva and
67 Siever, 1988). Such a force could cause displacement and/or fracturing in the host sediments
68 (Watts, 1978; Dewers and Ortoleva, 1990; Noiriel et al., 2010), diagenetic replacement (Minguez
69 and Elorza, 1994; Maliva and Siever, 1988), or even uplift the overburden (Gratier et al., 2012).
70 Notably, Hilgers and Urai (2005) argued that crystallization pressure in fibrous quartz, calcite,
71 and gypsum veins was responsible for the arrangement of wall-rock inclusions within fibrous
72 veins, not a crack-seal mechanism as commonly advocated previously to their study. We build
73 on their pioneering contribution and analyze textures and crystal morphological characteristics of
74 fibrous calcite veins to argue that force of crystallisation can best explain the widening of these
75 veins during growth.

76 We report the results of field, petrographic, and SEM-EBSD examination of calcite beef veins in
77 the Lower Jurassic Charmouth Mudstone of the Wessex Basin, southern UK. It has been
78 suggested that initiation of calcite veins exposed in the study area was caused by overpressure
79 due to hydrocarbon generation during basin inversion in the early Cenozoic (Zanella et al.,
80 2015a). Meng et al. (2017) proposed that vein initiation could be attributed to generation of
81 methane gas during early burial of the host sediments, based on evidence from stable-isotope
82 compositions of the veins. The scope of the present paper is not to discuss the initial opening
83 mechanism of the beef veins, but to focus on how the veins became widened as a subsequent
84 process of fracture development. Through analysis of multiple lines of evidence for a displacive
85 mode of widening in the unconsolidated shales during burial, it has been possible to evaluate the
86 controls on calcite precipitation by the force of crystallization. The aims of this paper are (1) to
87 derive evidence for displacive widening from vein geometry texture and associated host-rock

88 deformation; (2) to investigate the relationship between preferred crystallographic orientations of
89 calcite and the paleostress state; (3) to obtain a better understanding of the widening mechanism
90 of calcite beef veins and the fibrous habit of calcite crystals. These vein systems presented allow
91 a fundamental study of the mineralization process of authigenic carbonate as fibrous veins, the
92 associated changes in the paleostress states, and the kinematics of rock deformation during vein
93 widening. We believe that the results are applicable to many other bedding-parallel vein sets in
94 sedimentary basins worldwide.

95 **THE CHARMOUTH MUDSTONE**

96 The calcite beef veins were investigated and sampled in the onshore outcrops of the Lower
97 Jurassic Charmouth Mudstone in Southern Dorset, UK (Fig. 1A). The E-W-striking cliffs expose
98 an entire Jurassic succession of the Wessex Basin. This interval contains all of the potential
99 source rocks for hydrocarbon resources in this region (Ruffell and Wignall, 1990; Coe, 1992;
100 Macquaker and Gawthorpe, 1993; Williams et al., 2001) (Fig. 1B). The Lower Jurassic
101 Charmouth Mudstone (Lower Lias) consists of dark gray laminated shales and mudstones, with
102 locally concretionary and tabular limestone beds that make up about 3% of the total volume
103 (Gallois and Paul, 2009). The sediments were deposited in an epeiric sea during the major
104 transgression at the end of Triassic (Anderton et al., 1979). The underlying Blue Lias Formation
105 passes into the Charmouth Mudstone Formation with a marked upward decrease in frequency,
106 thickness, and lateral persistence of limestone beds (Cox et al., 1999; Barton et al., 2011). Seams
107 of calcite beef veins are common in the shales of the Charmouth Mudstone, which is highly
108 fossiliferous and also organic-rich (TOC up to 10.4%) (Ebukanson and Kinghorn, 1986; Jenkyns
109 and Weedon, 2013; Zanella et al., 2015a). The shales exposed in the study area are immature,

with a maximum burial depth of 900 - 1100 m and a equivalent virtrinite reflectance of only 0.35% (Ebukanson, 1985).

METHODS

Vein geometry, size, and interaction were characterized in field investigation. Characterization of host-rock deformation focused on tip regions and overlapping zones of the veins. Representative vein samples were collected and cut into thin sections perpendicular to vein planes. An integrated optical and scanning electron microscopy (SEM) petrographic characterization method was used to reveal the composition, texture, and crystallographic information of the calcite veins and solid inclusions. The crystallographic orientations of calcite were measured using an electron backscatter diffraction (EBSD) detector attached to the SEM. The thin sections were mounted on a stage that was tilted at 70° with the median lines of calcite veins parallel to the x-axis of the SEM stage. The acquisition of electron backscatter patterns (EBSPs) was performed at 20 kV accelerating voltage and a working distance of 10 mm. To obtain optimal EBSPs, the thin sections were not coated with a conductive layer and a low-vacuum mode was adopted. A copper tape was attached to surfaces of the thin sections to reduce charging effects. EBSD and secondary electron data were automatically collected using Aztec software package. The EBSD data were then analyzed using HKL Channel 5 software package for orientation mapping and lattice-pole plotting (Humphreys, 2004). Orientation maps are presented using Y direction inverse pole figure (IPF) orientation maps by assigning a color to each of the corners of the IPF. Y direction is true vertical, thus the maps show color indexed to crystallographic orientations that lie along vertical direction. The *c*-axes are presented in lower-hemisphere, equal-area stereographic projections.

FIELD DATA

Geometry and Size

The calcite beef veins in the study area are predominantly bedding-parallel, exhibiting a white or gray color in sharp contrast to the enclosing black shales (Fig. 2). The veins consist of calcite crystals arranged perpendicular to vein planes, and a dark median zone of solid inclusions. Individual isolated veins commonly exhibit a lenticular shape with two gently tapering tips (Fig. 2C), allowing measurement of vein size upon the exposure surface. The veins range from several millimeters up to 2 meters in length, and ~ 1 millimeter to 1.5 cm in aperture. The aspect ratio (length/aperture) of single veins varies from 3.6 to 38.6 (N = 240) (Fig. 3), with an average value of 12.1.

Surface Morphology

Slabs of the beef veins often weather out, exposing morphologies in both cross-section view and plan view (Fig. 4). The vein surfaces are generally flat and smooth; however, circular ridges with a relief up to 5 mm protrude into the enclosing shale (Fig. 4A - D). The depressions between the ridges are filled with clays. Similar features have been reported by Marshall (1982). Such ridges commonly coexist with impurities of host-rock fragments trapped in the fibrous parts of veins. The radii of the ridges are approximately equal to the length of the fragments.

Interestingly, well-preserved fossil ammonites are observed on the surfaces of many beef veins (Fig. 4E-H). The morphologies of ammonites on both the upper and lower surfaces are symmetrical and separated by vertical calcite fibers. Single veins commonly contain large numbers of ammonites with varied sizes that are scattered on vein surfaces. Similar features were

153 also observed in the Lower Jurassic shales of the Neuquen Basin, Argentina (Rodrigues et al.,
154 2009).

155 ***Tip Structure***

156 The tip structures of calcite beef veins exhibit varied geometries. Single isolated veins commonly
157 contain tapering tips with narrow tip angles. These veins exhibit a spindle-like, symmetric shape
158 with the maximum aperture appearing in vein center, gradually decreasing towards vein tips (Fig.
159 4C). Other veins exhibit rather blunt tips and commonly appear in tight clusters (Fig. 6). The
160 blunt tips are wedge, round, or even square shaped with varying tip angles. Blunt tips in the
161 overlapping zones of adjacent vein commonly exhibit a planar-concave shape, with the outer
162 walls being consistently planar (Fig. 6C - D).

163 Beef veins with clear margins and regularly shaped tips were selected for the measurement of tip
164 angles. The measurement of vein aperture versus tip angle reveals no clear correlation between
165 vein aperture and tip angle (Fig. 5A). Eighty-seven percent of the tip angles (N = 175) are
166 between 5° and 25° (Fig. 5B), with an average value of 16.6°.

167 ***Vein Interaction***

168 Vein interactions are commonly observed in closely spaced vein sets, which are represented by
169 the change of vein aperture in the overlapping zones (Fig. 6). Fig. 6A illustrates a representative
170 example of vein interaction that is typically seen at outcrop in the study area. The upper vein
171 exhibits a planar tapering tip and a curved median zone, whereas the lower vein contains blunt
172 tips and a horizontal planar median zone. The median zone of the upper vein exhibits a curved
173 trace only in the overlapping zone, which is subparallel to the upper plane of the lower vein. The

aperture of the upper vein decreases gradually in the overlapping zone, corresponding to the increase in the aperture of the lower vein. Interestingly, the sum of aperture of the two veins remains approximately constant across the zone of overlap.

A similar example of vein interaction in closely spaced veins is illustrated in Fig. 6B. The only notable difference is the consistently planar median zones in all veins. Vein interactions are also commonly evident in the tips by a decrease in vein aperture accompanying planar median zones. Vein intersections and crosscutting relationships were not observed.

Host-Rock Deformation

The host rock enclosing calcite beef veins exhibits both brittle and soft deformation within the tip regions and overlapping zone, the styles of which shed light on (1) the extent of deformed rocks and compaction due to vein widening; (2) the rock mechanical properties and stress state when the veins were formed (Maher et al., 2016); and (3) the relative timing of neighboring veins. Fig. 6E shows typical host-rock deformation around beef veins. The shale laminae follow vein margins, which are gently folded where the vein aperture changes. Shear fractures with a reverse displacement are often developed in the tip regions of beef veins where the maximum curvature of vein margins appears.

Interpretation of Field Observations

The shale laminae lateral to vein tips are predominantly horizontal, whereas the corresponding laminae above or below the beef veins are displaced to their positions above or below their lateral correlatives (Fig. 6A, C). Such a displacement is interpreted to be caused by fiber vertical

194 growth. The extent of plastic deformation is restricted to within a limited range of centimeters
195 from the vein margins.

196 Fig. 7A illustrates the reconstruction of vein interaction and the associated deformation processes
197 in the host shales. The lower vein is interpreted to have ended before the upper vein, based on the
198 comparatively regular shape of the lower vein. It is further interpreted that the widening of the
199 lower vein caused vertical compaction in the enclosing clays with the laminae gently folded to
200 accommodate the expansion. This implies that the compaction state at the time of deformation
201 must have been such that localized additional compaction was possible due to vein widening,
202 analogues to the displacive effect on laminae observed around early formed, displacive nodules
203 (Watts, 1978; Lash and Blood, 2007). The curvature of the median zone of the upper vein is
204 thereby related to the curvature of the host bedding during the initiation of the upper vein. The
205 formation of the upper vein commenced along the curved bedding fissure at some time during
206 the continued widening of the lower vein. The extent of rock deformation is mainly restricted
207 within the overlapping areas of the two veins. The shale between the two veins has experienced
208 the highest degree of growth-related compaction.

209 The veins shown in Fig. 6B are interpreted to have ended simultaneously, so that the vertical
210 growth of fibers in the lower veins and the upper vein does not cause bending of the median
211 zones (7B). Folding of shale laminae is mainly restricted to the tip regions of veins. The shales
212 entrapped between the upper and lower veins have experienced symmetrical squeezing by the
213 upper and lower veins.

214 Reconstruction of the typical plastic and brittle deformations around vein tips, especially blunt
215 tips, is illustrated in Fig. 7C. Two veins are interpreted to have nucleated in two different but

closely spaced horizons. Fiber growth in both veins caused vertical compaction of both the upper and lower shales and finally led to shear fracturing in the tip region with the maximum curvature. The shales in the overlapping zone of two veins have suffered compressive stresses from both the veins. The displacive widening of the veins is highlighted by the folds in the tip regions and correlative laminae that mark the widening-related displacement of the shales.

PETROGRAPHY

The petrographic analysis of calcite beef veins is focused on crystal morphology, arrangement and textural patterns of the median zone and fibrous zones.

Median Zone

The calcite beef veins contain a thin band of dark median zone which is generally bedding-parallel (Fig. 8). Multiple discrete host-rock fragments are commonly present in the median zone, with the long dimension ranging from tens of micrometers to 2 mm (Fig. 8B, C). The host-rock fragments are gently dipping, with both ends linking with the median zone bands that lie in different levels, resulting in an overlap between the two median zones. Because median zones of antitaxial veins have been suggested as the nucleation sites of fractures (Bons and Montenari, 2005), the overlapped median zones in single beef veins are interpreted as simultaneously generated en echelon fractures that have been subsequently cemented by calcite. Meanwhile, the rock fragments between the initial fractures have been preserved in-situ and slightly rotated during fiber growth. Similar features of host-rock deformation associated with fiber growth have also been reported by Cobbold et al (2013).

SEM images demonstrate that the host-rock fragments of argillaceous materials that are scattered in the median zones are thinly laminated (Fig. 9). The clay laminae are generally subhorizontal where the contacting calcite crystals have planar, horizontal crystal faces. However, the clay laminae are gently or even intensely folded where some calcite crystals protrude into the clays (Fig. 9C - F). Importantly, the laminae are approximately parallel to the contacting faces of calcite. Shear fractures are commonly developed where the laminae exhibit maximum curvature.

Fibrous Zone

The beef veins consist of two fibrous zones on either side of the median zone (Fig. 8). The calcite fibers are parallel-aligned and closely packed, with almost no host-rock inclusions entrapped between neighboring fibers. Single fibers have gently tapering tips towards the median zone. The maximum fiber lengths are commonly constant on the same side of the median zone, which can be either similar to or significantly different from those on the opposite side.

It is common to observe blocky zones that are enclosed by calcite fibers (Fig. 10). The blocky zones here refer to the regions within calcite beef veins that consist of numerous, small and equant calcite crystals and host-rock inclusions (Fig. 10B). Two main types of blocky zones are identified, both of which have characteristic shapes. One type of blocky zone is circular in 2D, with a maximum diameter of 5 cm (Fig. 10A - C). These blocky zones are associated with ridges on vein surfaces. Deformation twins are found in the upper calcite fibers that are in contact with the blocky zones (Fig. 10C). It is notable that the upper fibers end where they encounter the blocky zone. The fibers below the blocky zones also exhibit tapering tips that point towards the blocky zone. Hence, the fibers below the blocky zones are newly nucleated crystals rather than truncated fibers during the incorporation of host-rock inclusions.

The other type of blocky zone exhibits a conical shape, and consists of both small and equant calcite crystals along the cone margins and fibers in the center (Fig. 10E - H). Fibers outside the cones end where they encounter the cones rather than penetrating them. Conical blocky zones contain linear, subhorizontal bands of host-rock inclusions with widely disseminated pyrite microcrystals and organic-matter patches. Such cones are considered unlikely to be cone-in-cone structures, because (1) cone-in-cone structures consist of nested cones of fibrous calcite, regardless of cone sizes (e.g., Tarr, 1922; Franks, 1969; Cobbold and Rodrigues, 2007; Cobbold et al., 2013), whereas the conical blocky zones presented here contain equant, blocky calcite crystals; (2) the veins would be expected to exhibit a more homogeneous distribution of pyrite and organic matter, if the conical blocky zone was a cone-in-cone structure, because cone-in-cone structures and fibrous veins have been suggested to share similar formation mechanisms (Marshall, 1982; Cobbold and Rodrigues, 2007); and (3) the circular blocky zones exhibit compositions and fabrics similar to those of the conical blocky zones, indicating that the two types of blocky zones presumably have a similar origin.

The blocky zones presented here are interpreted to be remains of fossil skeletons. The fossil species possibly include ammonites, gastropods, and belemnites, which are prevalent in the Liassic shales (Jenkyns and Weedon, 2013), based on the distinct internal textures and compositions. The pyrite is likely to have formed during bacterial decomposition of organic tissues of the fossils. Inclusions of organic matter and some traces of the original shell texture have been retained, whereas the aragonitic shell constituents have been replaced by neomorphic calcite crystals. The high mechanical strength of the shells has prevented the fossils from distortion and being crushed by fiber growth. The appearance of twins in fibers shown in Fig. 10C indicates an intercrystalline deformation. Those twins are interpreted to have formed as

281 growth twins when fibers encountered rigid obstacles of fossil shells, because twinning is only
282 observed within fibers around the blocky zones. The fossil chambers may have served as sites of
283 fluid storage, allowing the precipitation of blocky calcite crystals in an open space. This explains
284 the different crystal morphology of precipitated calcite in the blocky zones as compared to the
285 neighboring fibrous zones. The incorporation of the skeletal fragments into fibrous zones of beef
286 veins is interpreted to have commenced during incremental growth of fibers rather than being
287 forced into fibers as a post-growth phenomenon.

288 ## EBSD ANALYSIS

289 The EBSD analysis of calcite beef veins focuses on quantitative measurement of the
290 crystallographic *c*-axis orientations and sizes of calcite crystals in the calcite beef veins,
291 providing evidence for the growth mechanism of calcite crystals.

292 ### *Fibers*

293 A representative fibrous zone of a beef vein is illustrated in Fig. 11A. In general, it is observed
294 that the fibers have a preferred *c*-axis orientation in the direction perpendicular to vein planes
295 (Fig. 11B). To examine the subtle variations in *c*-axis preferred orientations (CPO) of calcite
296 fibers from the median zone towards vein margins, the upper fibrous part of the vein is
297 subdivided into four zones for *c*-axis stereonet projections. The results reveal a trend of increase
298 in vertical *c*-axis CPO away from the median zone (Fig. 11C). In zone I, the calcite crystals
299 cover a much wider range of *c*-axis orientations than the other zones. Numerous small and
300 blocky crystals are present in the median zone, exhibiting nearly random *c*-axis orientations. The
301 plunges of *c*-axes in zones II and III ranges from 50° to 90°. The lowest plunge of *c*-axis is 40°.
302 In zone IV, the *c*-axes of crystals mainly plunge at 60 - 90°. Hence, *c*-axis CPO of calcite

303 gradually increases from the median zone towards vein margins to be closely clustered in the
304 vertical direction.

305 It is notable that individual fibers rarely extend from the median zone to vein margins (Fig. 12D).
306 Fiber overgrowth occurs frequently between neighboring fibers, leading to the termination of
307 some crystals, especially those with low *c*-axis plunges. Single fibers commonly exhibit a
308 lenticular geometry and a sharp tip with the apices pointing towards the median zone.
309 Orientations of *c*-axes are constant in single fibers, which are not necessarily coincident with the
310 long-axis orientations.

311 ***Blocky Zones***

312 The blocky zones within the fibrous parts of beef veins share similar features of crystal shape,
313 size, and *c*-axis fabric, which are in marked contrast to the enclosing fibers (Fig. 12). The calcite
314 crystals are predominantly small and equidimensional, exhibiting randomly oriented *c*-axes. The
315 crystals close to host-rock inclusions are tightly clustered and exhibit a mosaic fabric. However,
316 the fibers in the center of the conical blocky zone have subvertical *c*-axes that are similar to those
317 outside the cone.

318 ***Tip Structure***

319 Tips were sampled at the edges of veins. Fig. 13A shows a representative tip structure of a
320 calcite beef vein. It is notable that the median zone band is absent in the most frontal part of the
321 tip. The tip contains both equant and elongate-fibrous crystals of calcite (Fig. 13B). The equant
322 crystals exhibit varied sizes and are localized mainly along vein margins. The elongate-fibrous

crystals are orthogonal to the upper wall, with a plunge of 60°. The stereonet projections of *c*-axes of calcite reveal a CPO with *c*-axis plunges clustered between 60° and 80° (Fig. 13D).

DISCUSSION

Vein Displacive Widening by Force of Crystallization

The prevalent soft deformation in the shales around the calcite beef veins suggests that the sediments should be semilithified with a relatively high porosity. From this condition it is inferred that the authigenic growth of fibrous calcite crystals would have been capable of inducing growth-related soft-sediment deformation in the adjacent shales. More evidence for the timing hinges on the delicate fossil structures that have been so well preserved on vein surfaces. The high degree of fossil preservation indicates (1) a rapid rate of deposition so as to avoid surface weathering (Potter et al., 2005); and (2) cementation in fossil chambers predating actual compaction of the host sediments, which inhibits the mechanical crushing (Selles-Martinez, 1996). Moreover, the fold-related shear fractures in the host shales in vein-tip regions presumably indicate a transition from soft to later brittle deformation during incremental expansion of the veins (Maher et al., 2016). Hence, it is suggested the widening of veins commenced during the early stages of burial before any significant consolidation or cementation of the sediments.

The calcite fibers are interpreted here to exhibit a displacive widening as opposed to a passive cementation of voids. This interpretation is based on the following field and petrographic evidence:

(1) The distinctive morphology and *c*-axis fabrics of calcite fibers suggest a contrasting growth mode of fibers compared to the crystals cementing the blocky and median zones.

(2) The presence of split and displaced fossils with impressions preserved on both surfaces of single veins demonstrates that the fossils were separated by calcite fibers.

(3) The localized compaction and folding of the surrounding clay flakes in vein overlapping zones in Figs 6A and 10 show the impact of crystallization on host-rock deformation. The deformation is unlikely to be caused by differential compaction of muds around the lower vein in Fig. 6A, because the laminae above the upper vein are planar and horizontal.

(4) The square ends of some veins represent the shear surfaces separating the displaced and nondisplaced areas.

(5) The incorporation of detrital clasts and fossil skeletons, during fiber vertical growth, is interpreted to have occurred at a rate that matches the rate of fiber growth, so that the spaces between those inclusions and fibers could remain limited enough to eliminate growth competition of calcite crystals and allow them to adopt a fibrous habit, as suggested by Bons and Montenari (2005).

It has been demonstrated that calcite crystals can grow displacively and exhibit distinct neomorphic fabrics (Watts, 1978). The displacive growth of calcite was recognized from the occurrence of split fossils (Brown, 1954; Woodland, 1964; Marshall, 1982), from the disruption and brecciation of detrital fragments (Watts, 1978; El-Shahat and West, 1983; Maliva and Siever, 1988), from displacement and incorporation of host sediment particles (Woodland, 1964), and from the texture of the compacted domains of the clay matrix separated by calcite crystals (Astin and Scotchman, 1988). It has even been argued that displacive growth of calcite is capable of uplifting the overburden (Wiltschko and Morse, 2001; Gratier et al., 2012). Although displacive

366 calcite has frequently been described, the implications of this process have been largely ignored
367 (Watts, 1978).

368 It has been suggested that fibrous growth of calcite in black shales could be possible only if the
369 bedding planes were held apart against the confining pressure by fluid pressure (Parnell et al.,
370 2000). Under such conditions, the clay films could have been injected into the spaces between
371 adjacent cones by fluids (Selles-Martinez, 1994). However, it is difficult to explain the retained
372 clay laminae as well as their uniform orientations, which are parallel to the faces of fiber ends, in
373 the event that they were injected by advective flow. Zanella et al. (2015a) suggested that
374 overpressure caused by oil generation could be responsible for the development of the calcite
375 veins, based on the finding of patches of organic matter within the veins. However, the organic
376 matter in the host shales is not mature enough to generate oil (Ebukanson, 1985) and subsequent
377 overpressuring in the host rock. The aspect ratio of mineral veins as hydrofractures has been used
378 to evaluate the static overpressure of the fluid, Δp, (Gudmundsson, 1999; Philipp, 2012):

$$\Delta p = \frac{AE}{2L(1-v^2)}$$

379 Where E is the Young's modulus of the rock within which the vein occurs; v is the Poisson's
380 ratio; and A and L are the aperture and length of the vein respectively. Hence, given a certain
381 overpressure in the sediments, a constant aspect ratio of resulting veins could be inferred,
382 regardless of their sizes. However, the non-uniform vein aspect ratios of beef veins presented in
383 this study suggest that fluid pressure may not fully explain the varied vein sizes and geometries.
384 The nonlinear aperture-to-length relationship could be induced by mechanical vein interactions
385 (Olson, 2003), which are commonly observed in vein overlapping zones and tip regions.

386 The value of crystallization pressure of calcite is largely determined by the degree of
387 supersaturaion of the pore fluid (Correns, 1949; Dewers and Ortoleva, 1990). In sea water, the
388 crystallization pressure of calcite may reach up to ~ 50 MPa at the degree of supersaturation of
389 2 (Wiltschko and Morse, 2001). The lines of evidence for displacive widening of calcite beef
390 veins strongly argues that the force of crystallization of calcite fibers is likely to be responsible
391 for the displacement of the host rocks and for creation of space for fiber growth (Fig. 14). This
392 neatly explains the absence of median zones in the most frontal parts of beef veins, where there
393 is an absence of evidence supporting hydraulic fracturing as a mechanism for lateral propagation
394 of veins. Displacive widening by force of crystallization is a better explanation because the
395 widening of the veins occurred during an early stage of compaction when the sediments were
396 still capable of being locally strained by additional plastic deformation. The spatial relationship
397 of neighboring veins presented in Fig. 6A suggests that folding of the wrap-around host-rock
398 laminae are induced by vein widening rather than by later differential compaction around the
399 beef vein.

400 The coupling of mineral growth kinetics and mechanical response of the host rocks has been
401 subdivided into three cases (Fletcher and Merino, 2001): (1) crystal growth by replacement in a
402 hydrostatically stressed elastic rock; (2) syntectonic crystallization in a rock undergoing bulk
403 pure shear; and (3) widening of veins accommodated by viscous relaxation of the host rock. Case
404 three is most compatible with our observations of beef veins in the black shales. The self-stress
405 by crystal growth will remain regardless of the external loads. Such a supersaturation-driven
406 stress could drive vein widening and propagation, accommodated by deformation of the
407 surrounding rocks (Taber, 1916; Fletcher and Merino, 2001; Means and Li, 2001; Wiltschko and
408 Morse, 2001).

409 The process of vein widening and associated host-rock deformation summarized in Fig. 7 can
410 best represent the role of force of crystallization in vein widening and also the incorporation of
411 host-rock inclusions into veins. This builds on a model for vein widening and continuous growth
412 advocated by Hilgers and Urai (2005). Their model attempted to explain the incorporation of
413 solid wall-rock inclusions into a fibrous vein, and they described field examples where echelon
414 crack growth in particular was argued to be indicative of continuous vein growth opened actively
415 by the force of crystallization (Hilgers and Urai, 2005, p485). To explain the process whereby
416 solid inclusions were incorporated into two neighboring veins, the authors favored a constant
417 growth rate along the vein to explain the incorporation process of such solid inclusions. In this
418 model, vein nucleation is suggested to occur diachronously. Widening of the later vein would
419 cause simple shearing in the wall rock between the two neighboring veins. Consequently, the
420 incorporation of the host-rock fragments would result from simultaneous vein widening that
421 would be finally enclosed by crystal fibers.

422 The Hilgers and Urai (2005) model offers a good general explanation for the textures we observe
423 in the Charmouth Mudstone. However, the precise details of their model may not be applicable
424 in this study, for the following reasons. Firstly, if we assume the veins have a constant growth
425 rate, vein thickness would then be expected to depend on the timing of vein nucleation. In this
426 case the thicker vein can either be the longer vein (Fig. 6A), or the shorter vein (Fig. 6B).
427 However, the shorter vein would be inevitably thinner than the longer vein in the model by
428 Hilgers and Urai (2005), due to the later timing and limited growth space of the shorter vein,
429 which is contrary to the case illustrated in Fig. 6A. Secondly, all of the solid inclusions in the
430 model are straight and could not satisfactorily explain the curved median lines in the veins
431 presented (Fig. 6A). Moreover, the continuous traces of shale laminae in the solid inclusions

between neighboring veins (Fig. 6A, B) suggest that the solid inclusions are intact without being subjected to simple shear. This indicates that the growth-related shale deformation is still plastic rather than brittle.

It is notable that the displacive growth of calcite fibers is not necessarily accompanied by a volumetric expansion of the bulk rock by uplifting the overburden. The crystallization of calcite is argued here to predate the full compaction of the host clays, which is evident from the undeformed fossils on beef surfaces. The expansion of the veins could therefore have been accommodated by an additional vertical compaction in the country rock (Franks, 1969). Such a localized strain is especially evident from vein tip regions. Furthermore, the sediments may even suffer a volume loss that is synchronous with diagenetic growth of the veins (Selles-Martinez, 1994). This is due to the mechanical compaction that causes rapid expulsion of pore water and a reduction in porosity of the sediments.

Orientations of c-axes

Given the crystal morphologies, sizes, and crystallographic orientations of calcite fibers that are different from those in the median zones and blocky zones, it is argued that these differently arranged crystals do not share the same growth mechanism. Blocky crystals have been suggested to form in fluid-filled vugs or fractures, where growth competition leads to some crystals overgrowing others (Durney and Ramsay, 1973). Such calcite crystals owe their random *c*-axis orientations to the hydrostatic stress under which precipitation occurred, whereas the calcite fibers grew under a nonhydrostatic stress. Previous studies suggested that the fibrous habit of minerals is the result of a lack of growth competition between neighboring crystals (Bons and Montenari, 2005). Crystals would exhibit a fibrous morphology if the crystals has a higher

potential growth rate than the widening rate of the veins (Bons, 2000; Hilgers et al., 2001). The question then arises about the origin of preferred orientations of calcite fibers and their *c*-axes.

Orientations of calcite fibers is suggested to be the function of the local environment and a response to the directions of easiest crystal growth (Franks, 1969). Mechanically, the crystal lattice tends to have a preferred crystal orientation along the elastically weakest axis under non-hydrostatic stresses (Kamb, 1959; Yoshida et al., 1996). This could minimize the chemical potential required for equilibrium for crystallization, due to the anisotropic properties of crystal lattice. Kamb's theory shows that the chemical potential of the nonhydrostatically stressed solid in contact with a fluid is given as

$$\mu = u - Ts - \sigma_n v$$

Where μ is the chemical potential of the solid component in the fluid, u is the molar internal energy of the solid, s is the molar entropy of the solid, σ_n is the normal stress acting on the interface, and v is the molar volume of the solid. Kamb (1959) extended the condition to the contact of two solids. The equilibrium condition of the stressed solid at the interface can be presented as

$$\mu_n(\omega) = u(\omega) - Ts(\omega) - \sigma_n v(\omega)$$

Where ω is the crystal orientation, and n is the orientation of the interface. Those grains in the orientations with the lowest chemical potential can grow the most. For calcite, the *c*-axis is the weakest axis, along which the crystallization of calcite is favored across the plane normal to the maximum principal stress σ_1 (Kamb, 1959; Milholland et al., 1980; Larson and Tullborg, 1984).

Hence, across a given interface between crystals and fluid, calcite grows the fastest with its *c*-axis aligned with σ_1.

This theory has been supported by the oriented nucleation of crystals with the distribution of *c*-axes as predicted (Shelley, 1977, 1980; Larson and Tullborg, 1984; Becker, 1995), and in experimentally deformed limestone (Wenk et al., 1973). The theory has also been used to interpret the origin of preferred vertical orientation in deep-sea pelagic carbonate sequences and the associated velocity anisotropy (Kim et al., 1983), stress-induced preferred orientation of iron crystals in the inner core (Yoshida et al., 1996), and preferred *c*-axis orientations in calcite cone-in-cone structures (Woodland, 1964; Franks, 1969). Additionally, calcite is the most stable in-situ with the *c*-axis parallel to σ_1 due to the preferential dissolution of calcite with *c*-axes not oriented to σ_1 under nonhydrostatic stresses (Adelseck et al., 1973; Carlson et al., 1983; O'Brien et al., 1993). Moreover, as discussed above, the generation of calcite beef veins is argued to commence at a shallow level during sediment burial and early diagenesis where a sub-vertical minimum principal stress σ_3 is unlikely. This infers a K_o loading condition, in which K_o is the ratio of the horizontal effective stress to the vertical effective stress and is often used to describe the stress conditions active during sediment burial (Jones and Addis., 1984, 1985; Bjorlykke and Hoeg, 1997). The value of K_o is normally less than 1 and is typically 0.6 for clays during burial (Lambe and Whiteman, 2008).

Hence, it is argued that the σ_1 was orthogonal to vein walls and promoted the growth of calcite with subvertical *c*-axis orientations. This σ_1 is due to gravity under the K_o loading conditions. The shape of growing crystals and the crystallization stresses act as cause and effect in the kinetic - rheological interaction attending crystal growth in rocks (Nabarro, 1940; Fletcher and Merino, 2001). In this view, the preferred subhorizontal orientation of the beef veins can be

attributed to the fact that the veins took advantage of weak planes of subhorizontal bedding fissures with a low tensile strength (Shearman et al., 1972).

Our study of fibrous calcite veins draws conclusions similar to those presented by Hilgers and Urai (2005) that the force of crystallization offers the best explanation for textural relationships involving fiber geometry and wall-rock inclusions in fibrous veins. In addition, our evidence from EBSD analyzes of *c*-axis orientations, and deformation of host-rock laminae, adds further weight to the general argument that fibrous, crudely bedding-parallel veins may grow in a continuous fashion by force of crystallization rather than by crack seal increments under an episodic fluid-overpressure driving condition. Since fibrous veins are so widely distributed in nature, our study adds to a growing number of documented cases where a strong case can be made that vein growth is driven by force of crystallization, and this may have major implications for how the structural and hydrodynamic context underpinning vein growth is perceived.

CONCLUSIONS

The subhorizontal calcite beef veins in the Lower Jurassic Charmouth Mudstone exhibit a displacive widening, as evident by (1) fossils separated by subvertical fibers; (2) vein interactions that caused decrease in vein aperture and folding of laminae; (3) soft deformation of host-rock fragments in the median zones of single beef veins; and (4) shear fracturing in the rocks around blunt vein tips and clay flakes protruded by fibers. The calcite fibers exhibit preferred *c*-axis orientations that are normal to vein walls, whilst calcite crystals in the median zones and blocky zones have nearly random *c*-axis orientations, suggesting the fibers grew under a nonhydrostatic stress. Given the displacive widening of fibers and their distinct *c*-axis orientations, the force of crystallization is suggested to be responsible for vein widening and also

517 for controlling the preferred growth of calcite fibers. This study suggests that bedding-parallel
518 calcite veins, which appear commonly in black shales in sedimentary basins, may become
519 widened by the induced stress of crystallization as a subsequent process of fracture sealing,
520 rather than by fluid overpressure that caused dilation in the rocks.

521 **ACKNOWLEDGEMENTS**

522 This research was funded by Shell International Exploration and Production B.V. We thank Jon
523 Wells for sample preparation. We also thank Lars Hansen and David Wallis for help with EBSD
524 and beneficial discussions. We are grateful for the insightful reviews by Alain Zanella and Janos
525 Urai. Leslie Melim and Sally Sutton are acknowledged for providing constructive comments and
526 manuscript editing. John Southard is thanked for technical editing of this paper.

527 **REFERENCES**

528 Adelseck, C. G., Geehan, G. W., and Roth, P. H., 1973, Experimental evidence for the selective
529 dissolution and overgrowth of calcareous nannofossils during diagenesis: Geological
530 Society of America, Bulletin, v. 84, p. 2755-2762.
531 Al-Aasm, I., Coniglio, M., and Desrocheres, A., 1995, Formation of complex fibrous calcite
532 veins in Upper Triassic strata of Wrangellia Terrain, British Columbia, Canada:
533 Sedimentary Geology, v. 100, p. 83-95.
534 Anderton, R., Bridges, P., Leeder, M., and Sellwood, B., 1979, Dynamic Stratigraphy of the
535 British Isles; A Study in Crustal Evolution: London, Allen & Unwin, 301p.
536 Astin, T., and Scotchman, I., 1988, The diagenetic history of some septarian concretions from
537 the Kimmeridge Clay, England: Sedimentology, v. 35, p. 349-368.

538 Barton, C., Woods, M., Bristow, C., Newell, A., Westhead, R., Evans, D., Kirby, G., and
539 Warrington, G., 2011, Geology of south Dorset and south-east Devon and its World
540 Heritage Coast: Special Memoir for 1: 50 000 geological sheets, British Geological
541 Survey, Keyworth.
542 Basson, I., and Viola, G., 2004, Passive kimberlite intrusion into actively dilating dyke–fracture
543 arrays: evidence from fibrous calcite veins and extensional fracture cleavage: Lithos, v.
544 76, p. 283-297.
545 Becker, A., 1995, Quartz pressure solution: influence of crystallographic orientation: Journal of
546 Structural Geology, v. 17, p. 1395-1405.
547 Bjorlykke, K., and Hoeg, K., 1997, Effects of burial diagenesis on stresses, compaction and fluid
548 flow in sedimentary basins: Marine and Petroleum Geology, v. 14, p. 267-276.
549 Bols, H. M. N., Hermanrud, C., and Teige, G. M. G., 2004, Origin of overpressures in shales:
550 Constraints from basin modeling: American Association of Petroleum Geologists,
551 Bulletin, v. 88, p. 193-211.
552 Bons, P. D., and Jessel, M. W., 1997, Experimental simulation of the formation fibrous veins by
553 localised dissolution - precipitation creep: Mineralogical Magazine, v. 61, p. 53-63.
554 Bons, P. D., 2000, The formation of veins and their microstructures: Journal of the Virtual
555 Explorer, v. 2, p. 1-47, doi:10.3809/jvirtex.2000.00007.
556 Bons, P. D., and Montenari, M., 2005, The formation of antitaxial calcite veins with well-
557 developed fibres, Oppaminda Creek, South Australia: Journal of Structural Geology, v.
558 27, p. 231-248.
559 Bons, P. D., Elburg, M.A., and Gomez-Rivas, E., 2012, A review of the formation of tectonic
560 veins and their microstructures: Journal of Structural Geology, v. 43, p. 33-62.

561 Brown, R. W., 1954, How does cone-in-cone material become emplaced?: American Journal of
562 Science, v. 252, p. 372-376.
563 Carlson, R., Schaftenaar, C., and Moore, R., 1983, Causes of compressional-wave anisotropy in
564 calcareous sediments from the Rio-grande rise: Initial Reports of the Deep Sea Drilling
565 Project, v. 72, p. 565-576.
566 Cobbold, P. R., and Rodrigues, N., 2007, Seepage forces, important factors in the formation of
567 horizontal hydraulic fractures and bedding-parallel fibrous veins ('beef' and 'cone-in-
568 cone'): Geofluids, v. 7, p. 313-322.
569 Cobbold, P. R., Zanella, A., Rodrogues, N., and Loseth, H., 2013, Bedding-parallel fibrous veins
570 (beef and cone-in-cone): worldwide occurrence and possible significance in terms of
571 fluid overpressure, hydrocarbon generation and mineralization: Marine and Petroleum
572 Geology, v. 43, p. 1-20.
573 Coe, A. L., 1992, Unconformities within the Upper Jurassic of the Wessex Basin, southern
574 England: Doctoral dissertation, University of Oxford, 240p.
575 Correns, C.W., 1949, Growth and dissolution of crystals under linear pressure: Discussions of
576 the Faraday society, v. 5, p. 267-271.
577 Cox, B., Sumbler, M., and Ivimey-Cook, H., 1999, A Formational Framework for the Lower
578 Jurassic of England and Wales (Onshore Area): Research report RR/99/001, British
579 Geological Survey, 25p.
580 Dewers, T., and Ortoleva, P., 1990, Force of crystallization during the growth of siliceous
581 concretions: Geology, v. 18, p. 204-207.

582 Durney, D. W., and Ramsay, J. G., 1973, Incremental strains measured by syntectonic crystal
583 growths, in De Jong, K.A., Scholten, K., eds., Gravity and Tectonics: New York, John
584 Wiley & Sons, p. 67-96.
585 Ebukanson, E., 1985, Kerogen facies in the major Jurassic mudrock formations of southern
586 England and the implication on the depositional environments of their precursors:
587 Journal of Petroleum Geology, v. 8, p. 435-462.
588 Ebukanson, E., and Kingborn, R., 1986, Maturity of organic matter in the Jurassic of Southern
589 England and its relation to the burial history of the sediments: Journal of Petroleum
590 Geology, v. 9, p. 259-280.
591 El-Shahat, A., and West, I., 1983, Early and late lithification of aragonitic bivalve beds in the
592 Purbeck Formation (Upper Jurassic - Lower Cretaceous) of southern England:
593 Sedimentary Geology, v. 35, p. 15-41.
594 Fisher, D. M., Brantley, S. L., Everett, M., and Dzvonik, J., 1995, Cyclic fluid flow through a
595 regionally extensive fracture network within the Kodiak accretionary prism: Journal of
596 Geophysical Research: Solid Earth, v. 100, p. 12,881-12,894.
597 Flemings, P. B., Liu, X., and Winters, W. J., 2003, Critical pressure and multiphase flow in
598 Blake Ridge gas hydrates: Geology, v. 31, p. 1057-1060.
599 Fletcher, R. C., and Merino, E., 2001, Mineral growth in rocks: kinetic - rheological models of
600 replacement, vein formation, and syntectonic crystallization: Geochimica et
601 Cosmochimica Acta, v. 65, p. 3733-3748.
602 Franks, P. C., 1969, Nature, origin, and significance of cone-in-cone structures in the Kiowa
603 Formation (Early Cretaceous), north-central Kansas: Journal of Sedimentary Petrology,
604 v. 39, p. 1438-1454.

605 Freed, R. L., and Peacor, D. R., 1989, Geopressured shale and sealing effect of smectite to illite
606 transition: American Association of Petroleum Geologists, Bulletin, v. 73, p. 1223-1232.

607 Gale J. F. W., Laubach, S. E. Olson, J. E., Eichhubl, P., and Fall, A., 2014. Natural fractures in
608 shale: A review and new observations: American Association of Petroleum Geologists,
609 Bulletin, v. 98, p. 2165-2216.

610 Gallois, R., and Paul, C., 2009, Lateral variations in the topmost part of the Blue Lias and basal
611 Charmouth Mudstone formations (Lower Jurassic) on the Devon and Dorset coast:
612 Geoscience in Southwest England: Proceedings of the Ussher Society, v. 12, p. 125-133.

613 Gratier, J. P., Frery, E., Deschamps, P., Royne, A., Renard, F., Dysthe, D., Ellouz-Zimmerman,
614 N., and Hamelin, B., 2012, How travertine veins grow from top to bottom and lift the
615 rocks above them: The effect of crystallization force: Geology, v. 40, p. 1015-1018.

616 Gudmundsson, A., 1999, Fluid overpressure and stress drop in fault zones: Geophysical
617 Research Letters, v. 26, p. 115-118.

618 Hedberg, H. D., 1974, Relation of methane generation to undercompacted shales, shale diapirs,
619 and mud volcanoes: American Association of Petroleum Geologists, Bulletin, v. 58, p.
620 661-673.

621 Hilgers, C., Koehn, D., Bons, P., and Urai, J., 2001, Development of crystal morphology during
622 unitaxial growth in a progressively widening vein: II. Numerical simulations of the
623 evolution of antitaxial fibrous veins: Journal of Structural Geology, v. 23, p. 873-885.

624 Hilgers, C., and Urai, J. L, 2005, On the arrangement of solid inclusions in fibrous veins and the
625 role of the crack-seal mechanism: Journal of Structural Geology, v. 27, p. 481-494.

626 Hobbs, P. R. N., Entwisle, D. C., Northmore, K. J., Sumbler, M. G., Jones, L. D., Self, S., Barron,
627 M., and Medkin, J. L., 2012, Engineering Geology of British Rocks and Soils: Lias
628 Group: Research Report OR/12/032, British Geological Survey, 323p.
629 Hooker, J. N., and Cartwright, J., 2016, Dolomite overgrowths suggest a primary origin of cone-
630 in-cone: Geological Magazine, p. 1-18, https://doi.org/10.1017/S0016756816000807.
631 Hooker, J, N., Cartwright, J., Stephenson, B., Silver, C. R. P., Alexander, J. D., and Hsieh, Y.,
632 2016, Fluid evolution in fracturing black shales, Appalachian Basin: American
633 Association of Petroleum Geologists, Bulletin, v. 101, p.1203-1238.
634 Humphreys, F., 2004, Characterisation of fine-scale microstructures by electron backscatter
635 diffraction (EBSD): Scripta Materialia, v. 51, p. 771-776.
636 Jenkyns, H. C., and Weedon, G. P., 2013, Chemostratigraphy (CaCO3, TOC, δ13Corg) of
637 Sinemurian (Lower Jurassic) black shales from the Wessex Basin, Dorset and
638 palaeoenvironmental implications: Newsletters on Stratigraphy, v. 46, p. 1-21.
639 Jones, M. E., and Addis, M. A., 1984, Volume change during sediment diagenesis and the
640 development of growth faults: Marine and Petroleum Geology, v. 1, p. 118-122.
641 Jones, M. E., and Addis, M. A., 1985, On changes in porosity and volume during burial of
642 argillaceous sediments: Marine and Petroleum Geology, v. 2, p. 247-253.
643 Jowett, E. C., Cathles, L. M. III., and Davis, B. W., 1993, Predicting depths of gypsum
644 dehydration in evaporitic sedimentary basins: American Association of Petroleum
645 Geologists, Bulletin, v. 77, p. 402–413.
646 Kamb, W. B., 1959, Theory of preferred crystal orientation developed by crystallization under
647 stress: The Journal of Geology, v. 67, p. 153-170.

Kim, D. C., Katahara, K. W., Manghnani, M. H., and Schlanger, S. O., 1983, Velocity and attenuation anisotropy in deep-sea carbonate sediments: Journal of Geophysical Research: Solid Earth, v. 88, p. 2337-2343.

Kiriakoulakis, K., Marshall, J., and Wolff, G., 2000, Biomarkers in a Lower Jurassic concretion from Dorset (UK): Journal of the Geological Society, v. 157, p. 207-220.

Lahann, R. W, and Swarbrick, R. E., 2011, Overpressure generation by load transfer following shale framework weakening due to smectite diagenesis: Geofluids, v. 11, p. 362-375.

Larson, S. Å., and Tullborg, E. L., 1984, Stable isotopes of fissure-filling calcite from Finnsjön, Uppland, Sweden: Lithos, v. 17, p. 117-125.

Lash, G. G., and Engelder, T., 2005, An analysis of horizontal microcracking during catagenesis: Example from the Catskill delta complex: American Association of Petroleum Geologists, Bulletin, v. 89, p. 1433-1449.

Lash, G. G., and Blood, D. R., 2007. Origin of early overpressure in the upper devonian catskill delta complex, western New York state: Basin Research, v. 19, p. 51-66.

Lambe, T. W., and Whitman, R. V., 2008, Soil Mechanics, SI Version: New York, John Wiley & Sons, 553p.

Macquaker, J., and Gawthorpe, R., 1993, Mudstone lithofacies in the Kimmeridge Clay Formation, Wessex Basin, southern England: implications for the origin and controls of the distribution of mudstones: Journal of Sedimentary Research, v. 63, p. 1129-1143.

Maher H. D. JR, Ogata, K., and Braathen, A., 2016, Cone-in-cone and beef mineralization associated with Triassic growth basin faulting and shallow shale diagenesis, Edgeøya, Svalbard: Geological Magazine, v. 154, p. 201-216.

670 Maliva, R. G., and Siever, R., 1988, Diagenetic replacement controlled by force of crystallization:
671 Geology, v. 16, p. 688-691.
672 Marshall, J. D., 1982, Isotopic composition of displacive fibrous calcite veins: reversals in pore-
673 water composition trends during burial diagenesis: Journal of Sedimentary Research, v.
674 52, p. 615-630.
675 Means, W., and Li, T., 2001, A laboratory simulation of fibrous veins: some first observations:
676 Journal of Structural Geology, v. 23, p. 857-863.
677 Meng, Q., Hooker, J., and Cartwright, J., 2017, Early overpressuring in organic-rich shales
678 during burial: evidence from fibrous calcite veins in the Lower Jurassic Shales-with-
679 Beef Member in the Wessex Basin: Journal of the Geological Society, v. 174, p. 869-
680 882.
681 Milholland, P., Manghnanni, M. H., Schlanger, S. O., and Sutton, G. H., 1980, Geoacoustic
682 modeling of deep-sea carbonate sediments: Journal of the Acoustical Society of
683 America, v. 68, p. 1351-1360.
684 Minguez, J. M., and Elorza, J., 1994, Diagenetic volume-for-volume replacement: force of
685 crystallization and depression of dissolution: Mineralogical Magazine, v. 58, p. 135-142.
686 Nabarro, F., 1940, The influence of elastic strain on the shape of particles segregating in an alloy:
687 Proceedings of the Physical Society, v. 52, p. 90.
688 Noiriel, C., Renard, F., Doan, M. L., and Gratier, J. P., 2010, Intense fracturing and fracture
689 sealing induced by mineral growth in porous rocks: Chemical Geology, v. 269, p. 197-
690 209.

691 O'Brien, D. K., ManghnaniI, M. H., Tribble, J. S., and Wenk, H. R., 1993, Preferred orientation
692 and velocity anisotropy in marine clay-bearing calcareous sediments, in Rezak, R., and
693 Lavoie D. L., eds., Carbonate Microfabrics: Berlin, Springer, p. 149-161.
694 Oliver, N. H., and Bons, P. D., 2001, Mechanisms of fluid flow and fluid – rock interaction in
695 fossil metamorphic hydrothermal systems inferred from vein – wallrock patterns,
696 geometry and microstructure: Geofluids, v. 1, p. 137-162.
697 Olson, J. E., 2003, Sublinear scaling of fracture aperture versus length: An exception or the rule?:
698 Journal of Geophysical Research: Solid Earth, v. 108, 2413, p. 1-11.
699 Osborne, M. J., and Swarbrick, R. E., 1997, Mechanisms for generating overpressure in
700 sedimentary basins: a reevaluation: American Association of Petroleum Geologists,
701 Bulletin, v. 81, p. 1023-1041.
702 Parnell, J., and Carey, P. F., 1995, Emplacement of bitumen (asphaltite) veins in the Neuquén
703 Basin, Argentina: American Association of Petroleum Geologists, Bulletin, v. 79, p.
704 1798-1815.
705 Parnell, J., Blamey, N. J., Costanzo, A., Feely, M., and Boyce, A. J., 2014, Preservation of
706 Mesoproterozoic age deep burial fluid signatures, NW Scotland: Marine and Petroleum
707 Geology, v. 55, p. 275-281.
708 Parnell, J., Honghan, C., Middleton, D., Haggan, T., and Carey, P., 2000, Significance of fibrous
709 mineral veins in hydrocarbon migration: fluid inclusion studies: Journal of Geochemical
710 Exploration, v. 69, p. 623-627.
711 Philipp, S. L., 2012, Fluid overpressure estimates from the aspect ratios of mineral veins:
712 Tectonophysics, v. 581, p. 35-47.

713 Potter, P. E., Maynard, J. B., and Depetros, P. J., 2005, Mud and Mustones: Introduction and
714 Overview: Berlin, Springer Science & Business Media, 297p.
715 Ramsay, J. G., 1980, The crack-seal mechanism of rock deformation: Nature, v. 284, p. 135-139.
716 Rodrigues, N., Cobbold, P. R., Loseth, H., and Ruffet, G., 2009, Widespread bedding-parallel
717 veins of fibrous calcite ('beef') in a mature source rock (Vaca Muerta Fm, Neuquén
718 Basin, Argentina): evidence for overpressure and horizontal compression: Journal of the
719 Geological Society, v. 166, p. 695-709.
720 Ruffel, A., and Wignall, P., 1990, Depositional trends in the Upper Jurassic - Lower Cretaceous
721 of the northern margin of the Wessex Basin: Proceedings of the Geologists' Association,
722 v. 101, p. 279-288.
723 Selles-Martinez, J., 1994, New insights in the origin of cone-in-cone structures: Carbonates and
724 Evaporites, v. 9, p. 172-186.
725 Selles-Martinez, J., 1996, Concretion morphology, classification and genesis: Earth-Science
726 Reviews, v. 41, p. 177-210.
727 Shearman, D., Mossop, G., Dunsmore, H., and Martin, M., 1972, Origin of gypsum veins by
728 hydraulic fracture: Institution of Mining and Metallurgy, Transactions, Section B,
729 Applied Earth Science, v. 81, p. 149-155.
730 Shelley, D., 1977, Plagioclase preferred orientation in Haast schist, New Zealand: The Journal of
731 Geology, v. 85, p. 635-644.
732 Shelley, D., 1980, Quartz [0001]-axes preferred orientation, Bluff, New Zealand: origin
733 elucidated by grain-size measurements: Tectonophysics, v. 62, p. 321-337.
734 Sorby, H., 1860, On the origin of 'cone-in-cone': British Association for the Advancement of
735 Science, Report of the 29th Meeting, 1859. Transactions of Sections, Geology.

736 Stoneley, R., 1983, Fibrous calcite veins, overpressures, and primary oil migration: American
737 Association of Petroleum Geologists, Bulletin, v. 67, p. 1427-1428.
738 Taber, S., 1916, The growth of crystals under external pressure: American Journal of Science, v.
739 41, p. 532-556.
740 Tarr, W., 1922, Cone-in-cone: American Journal of Science, v. 21, p. 199-213.
741 Tarr, W., 1933, Origin of the "Beef" in the Lias Shales of the Dorset Coast: Geological
742 Magazine v. 70, p. 289-294.
743 Underhill, J. R., and Stoneley, R., 1998, Introduction to the development, evolution and
744 petroleum geology of the Wessex Basin, in Underhill, J. R., eds, The development,
745 evolution and Petroleum Geology of the Wessex Basin: Geological Society of London,
746 Special Publications, v. 133, p. 1-18.
747 Urai, J. L., Williams, P. F., and Van Roermund, H. L. M., 1991, Kinematics of crystal growth in
748 syntectonic fibrous veins: Journal of Structural Geology, v. 13, p. 823-836.
749 Watts, N., 1978, Displacive calcite: evidence from recent and ancient calcretes: Geology, v. 6, p.
750 699-703.
751 Wenk, H., Venkitasubramanyan, C., Baker, D., and Turner, F., 1973, Preferred orientation in
752 experimentally deformed limestone: Contributions to Mineralogy and Petrology, v. 38,
753 p. 81-114.
754 Weyl, P. K., 1959, Pressure solution and the force of crystallization: a phenomenological theory:
755 Journal of Geophysical Research, v. 64, p. 2001-2025.
756 Williams, C. J., Hesselbo, S. P., Jenkyns, H. C., and Morgans-Bell, H. S., 2001, Quartz silt in
757 mudrocks as a key to sequence stratigraphy (Kimmeridge Clay Formation, Late Jurassic,
758 Wessex Basin, UK): Terra Nova, v. 13, p. 449-455.

759 Wiltschko, D. V., and Morse, J. W., 2001, Crystallization pressure versus “crack seal” as the
760 mechanism for banded veins: Geology, v. 29, p. 79-82.
761 Woodland, B. G., 1964, The nature and origin of cone-in-cone structure: Fieldiana Geology, v.
762 13, p. 185-305.
763 Yoshida, S., Sumita, I., and Kumazawa, M., 1996, Growth model of the inner core coupled with
764 the outer core dynamics and the resulting elastic anisotropy: Journal of Geophysical
765 Research: Solid Earth, v. 101, p. 28,085-28,103.
766 Zanella, A., Cobbold, P. R., and Rojas, L., 2014a, Beef veins and thrust detachments in Early
767 Cretaceous source rocks, foothills of Magallanes - Austral Basin, southern Chile and
768 Argentina: Structural evidence for fluid overpressure during hydrocarbon maturation:
769 Marine and Petroleum Geology, v. 55, p. 250-261.
770 Zanella, A., Cobbold, P. R., and De Veslud, C., 2014b, Physical modelling of chemical
771 compaction, overpressure development, hydraulic fracturing and thrust detachments in
772 organic-rich source rock: Marine and Petroleum Geology, v. 55, p. 262-274.
773 Zanella, A., Cobbold, P. R., and Boassen, T., 2015a, Natural hydraulic fractures in the Wessex
774 Basin, SW England: Widespread distribution, composition and history: Marine and
775 Petroleum Geology, v. 68, p. 438-448.
776 Zanella, A., Cobbold, P. R., Ruffet, G. and Leanza, H. A., 2015b, Geological evidence for fluid
777 overpressure, hydraulic fracturing and strong heating during maturation and migration
778 of hydrocarbons in Mesozoic rocks of the northern Neuquén Basin, Mendoza Province,
779 Argentina: Journal of South American Earth Sciences, v. 62, p. 229-242.

780

781

782

783 **FIGURE CAPTIONS**

784 Fig. 1. A) Geological map of the study area and the distribution of outcrops of the Lias Group in
785 the UK. The arrow shows the study area on the coast of Dorset. Modified from Hobbs et al.
786 (2012). B) Jurassic stratigraphy of the Wessex Basin, UK. Modified from Underhill and Stoneley
787 (1998). The potential source rocks are highlighted in gray color.

788 Fig.2. Photographs showing the exposure of calcite beef veins in the Lower Jurassic shales in the
789 study area. A) A swarm of short subhorizontal beef veins. The camera cap is 5.2 cm in diameter.
790 B) Closely spaced calcite beef veins concentrated in a horizon. C) A lenticular beef vein with
791 gently tapering tips. The vein exhibits the maximum aperture in vein center. D) A closer view of
792 a calcite beef vein with a median zone and subvertical fibers. The coin in Parts C and D is 2.25
793 cm in diameter.

794 Fig. 3. A) Scatter plot of length versus aperture of calcite beef veins. B) Histogram showing the
795 distribution of aspect ratios of calcite beef veins. N = 240.

796 Fig. 4. Photographs showing circular ridges (A - D) and fossil skeletons (E - H) on surfaces of
797 calcite beef veins. A) A cluster of small circular ridges on the surface of beef vein. B) A circular
798 ridge and the corresponding host-rock fragment in a beef vein. C) A centimeter-scale sized
799 circular ridge in a beef vein. D) Dark host-rock inclusions in a beef vein and the associated
800 circular ridge. E) A beef vein exposing sub-vertical fibers and ammonite on the upper surface. F)
801 Plan view of a cluster of ammonites in varied sizes on vein surfaces. G) Plan view of a hand

802 specimen of a beef vein with well-preserved morphology of ammonite. H) Cross section of the
803 same beef vein in Part G showing the vertical fibers that separate fossil skeletons.

804 Fig. 5. A) Scatter plot of vein tip angles versus the maximum aperture of the veins. B) Histogram
805 showing the distribution of vein tip angles. N = 175.

806 Fig. 6. Photographs and their sketches showing the geometry and interaction of calcite beef veins
807 and the associated host-rock deformation. Red lines highlight the median zones. A) Two closely
808 spaced calcite beef veins. Note the decrease in aperture and the curved median zone of the upper
809 vein in the vein overlapping zone. B) Closely spaced beef veins. Note the decrease in aperture in
810 the vein overlapping zone and the straight median zones in all the veins. C) Soft and brittle
811 deformation in the tip overlapping zone of two beef veins. Note that the laminae are subparallel
812 to vein margins. D) Tips of two neighboring veins with gradually decreased aperture. Note that
813 the outer walls of the two veins remain planar. E) Soft deformation in the rocks around a blunt
814 vein tip. Shear fractures with a reverse displacement occur above the tip where the laminae
815 exhibit the maximum curvature. F) A cluster of short calcite beef veins in shales. The shale
816 laminae are subparallel to the contacting walls of beef veins.

817 Fig. 7. Sketch illustrating the growth process of closely spaced beef veins and growth-related
818 compaction in the host rocks See text for explanation. Frac = fracture. S = skeleton.

819 Fig. 8. A) Photomicrograph showing the texture and composition of a representative beef vein.
820 MZ = median zone. The median zone is subhorizontal. Note the upper fibers with decreased
821 length towards the right side of this figure (vein tip). B, C) occurrence of host-rock fragments in
822 the median zones of beef veins. HF = host rock fragment. MZ = median zone. Note the varied
823 levels on different sides of the host-rock fragment.

824 Fig. 9. SEM backscattered electron image showing the scattering of host-rock fragments and
825 their textures in beef veins. A) Multiple host rock fragments scattered in the median zone of a
826 beef vein. B) The enlarged area of the box in Part A. Note the well preserved bedding fissures in
827 the clay fragment. C) Folded clay laminae in a host-rock fragment due to the protruding of
828 calcite crystals. D) Curved and steep bedding of clay inclusions that is parallel to contacting
829 faces of calcite crystals. E) Gentle folding of clay laminae due to crystal protruding. F) Enlarged
830 area of the box in Part E. Note the occurrence of steep shear fractures. The dashed lines highlight
831 the bedding direction.

832 Fig. 10. The texture and composition of representative blocky zones in calcite beef veins. A)
833 SEM image showing a blocky zone with small, equant calcite crystals that exhibit significant
834 differences from the enclosing calcite fibers. B) Photomicrograph showing the area depicted in
835 Part A. Cross-polarized light. C) Enlarged area of the box in Part B showing the occurrence of
836 twinning in the calcite fibers that contact with the blocky zone. D) Conical blocky zones with
837 thinly laminated texture and also subvertical fibers in cone center. E) Photomicrograph showing
838 the area depicted in Part D. F) Enlarged area of the box in Part E showing the opaque
839 subhorizontal bands of organic matter in the conical blocky zone.

840 Fig. 11. A) Y-direction IPF coloring orientation maps (IPF-Y) showing the crystallographic
841 orientations of calcite fibers. B) Contoured stereonet projection of *c*-axis poles of the calcite
842 crystals in Part A. One data point per crystal. C) Stereonet projections of *c*-axis poles of the
843 crystals in the four different zones in Part A. D) IPF-Y map showing the crystallographic
844 orientations of four calcite fibers and the stereonet projections of their *c*-axis poles. Note that the
845 long-axis orientations of single fibers do not coincide with their *c*-axis orientations.

Fig. 12. IPF-Y maps showing the crystallographic orientations of the calcite crystals in A) rounded and B) conical blocky zones and the stereonet projections of their *c*-axis poles (right). See Parts C and E for optical images of the blocky zones.

Fig. 13. A) Photomicrograph showing a representative tip structure of a beef vein. Note the absence of the median zone in the frontmost part. B) IPF-Y map showing the crystallographic orientations of calcite in the box area in Part A. HR = host rock. BC = blocky crystal. C) Stereonet projections of calcite *c*-axis poles of all crystals in the box area in Part B, and D) the contoured projections showing the preferred orientations.

Fig. 14. Sketch illustrating the displacive growth of fibrous calcite veins in the tip region. Note that the median zone is absent in the decohesion region.

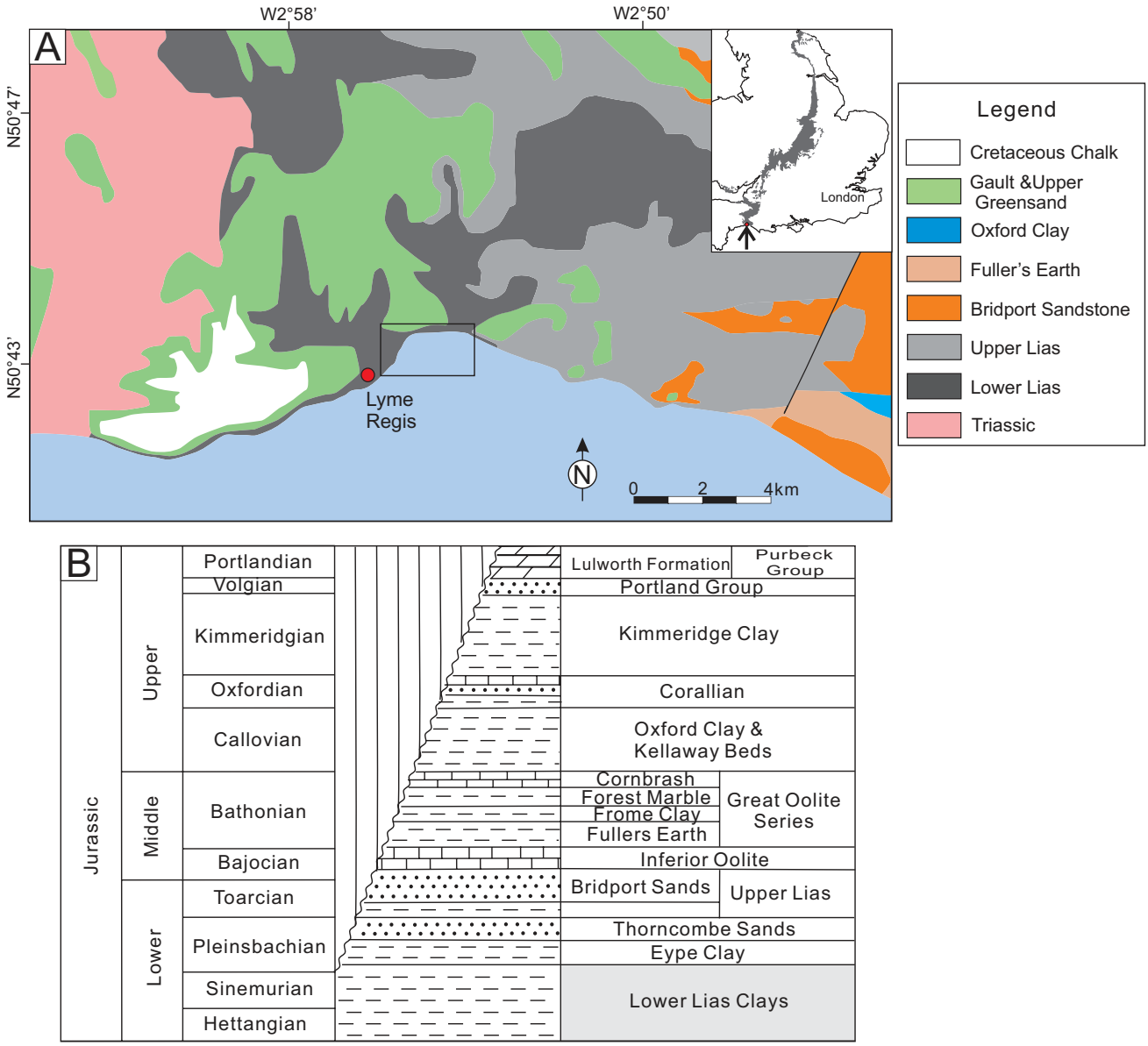
A
W2°58'
W2°50'
N50°47'
N50°43'
Lyme
Regis
London
N
0
2
4km
Legend
Cretaceous Chalk
Gault &Upper Greensand
Oxford Clay
Fuller's Earth
Bridport Sandstone
Upper Lias
Lower Lias
Triassic
B
Jurassic
Upper
Middle
Lower
Portlandian
Volgian
Kimmeridgian
Oxfordian
Callovian
Bathonian
Bajocian
Toarcian
Pleinsbachian
Sinemurian
Hettangian
Lulworth Formation
Purbeck Group
Portland Group
Kimmeridge Clay
Corallian
Oxford Clay &
Kellaway Beds
Cornbrash
Forest Marble
Frome Clay
Fullers Earth
Great Oolite Series
Inferior Oolite
Bridport Sands
Upper Lias
Thorncombe Sands
Eype Clay
Lower Lias Clays

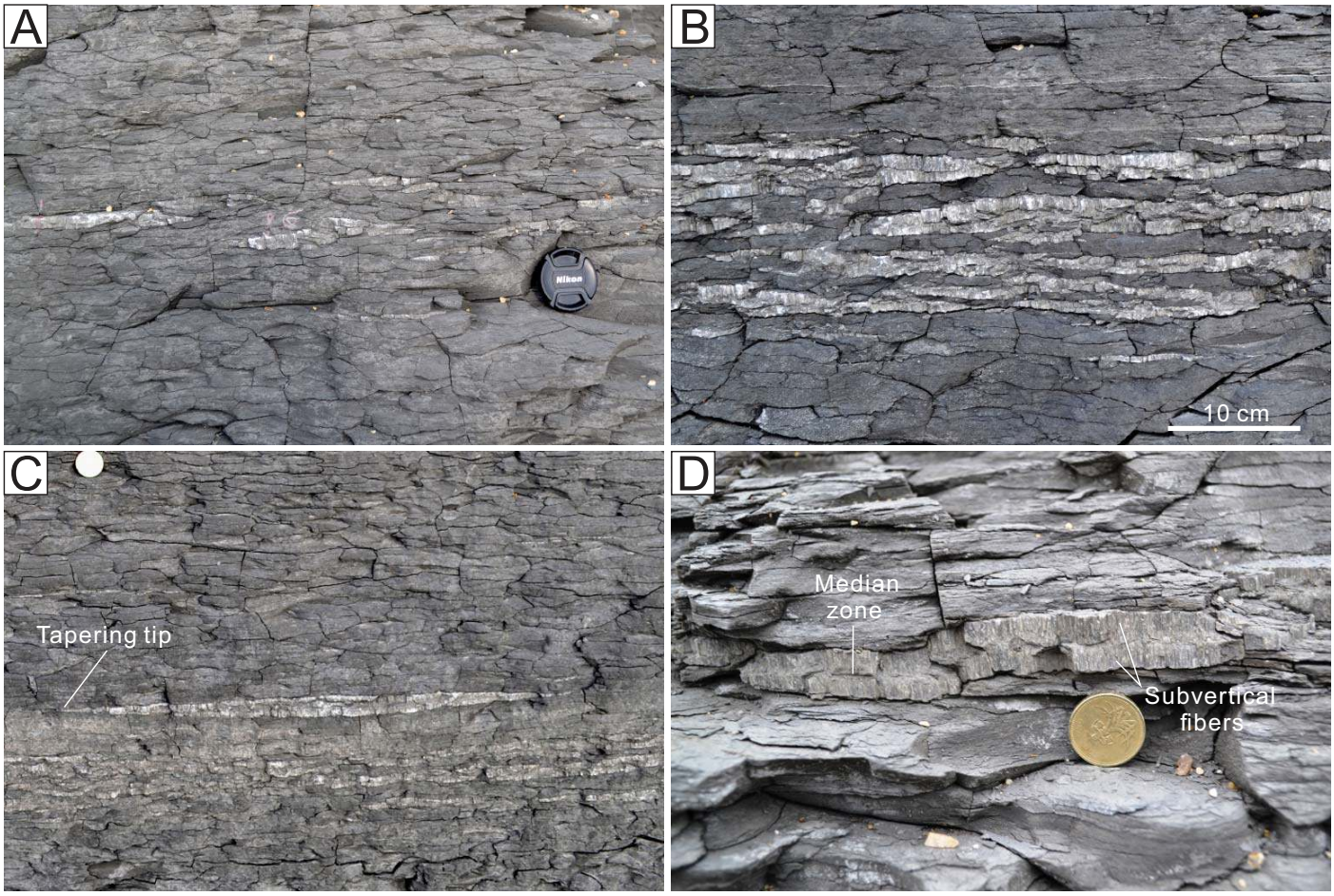
A
B
10 cm
C
Tapering tip
D
Median zone
Subvertical fibers

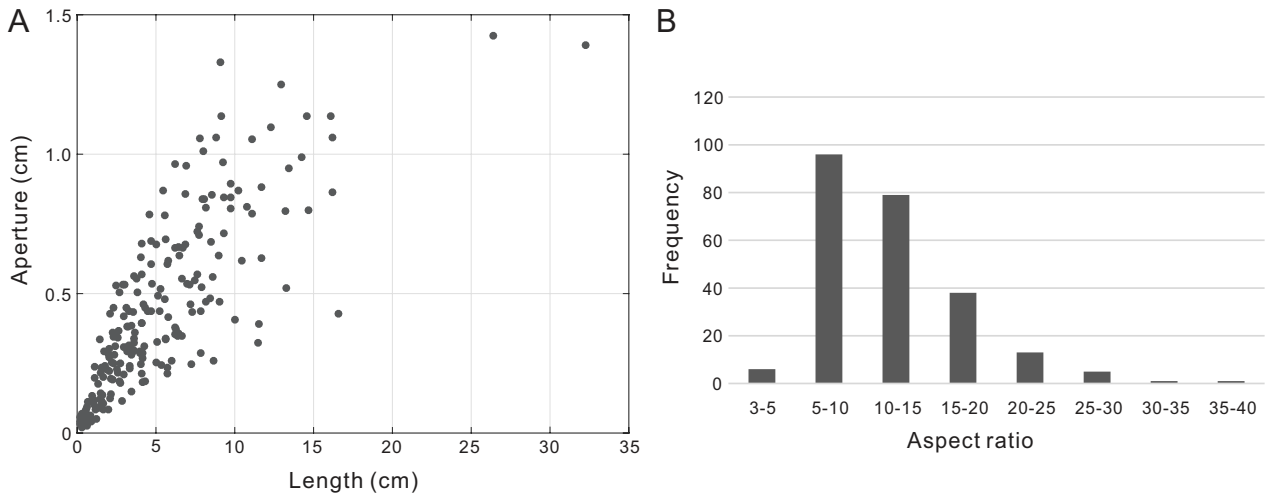
A
Aperture (cm)
Length (cm)
0
0.5
1.0
1.5
0
5
10
15
20
25
30
35
B
Frequency
Aspect ratio
0
20
40
60
80
100
120
3-5
5-10
10-15
15-20
20-25
25-30
30-35
35-40

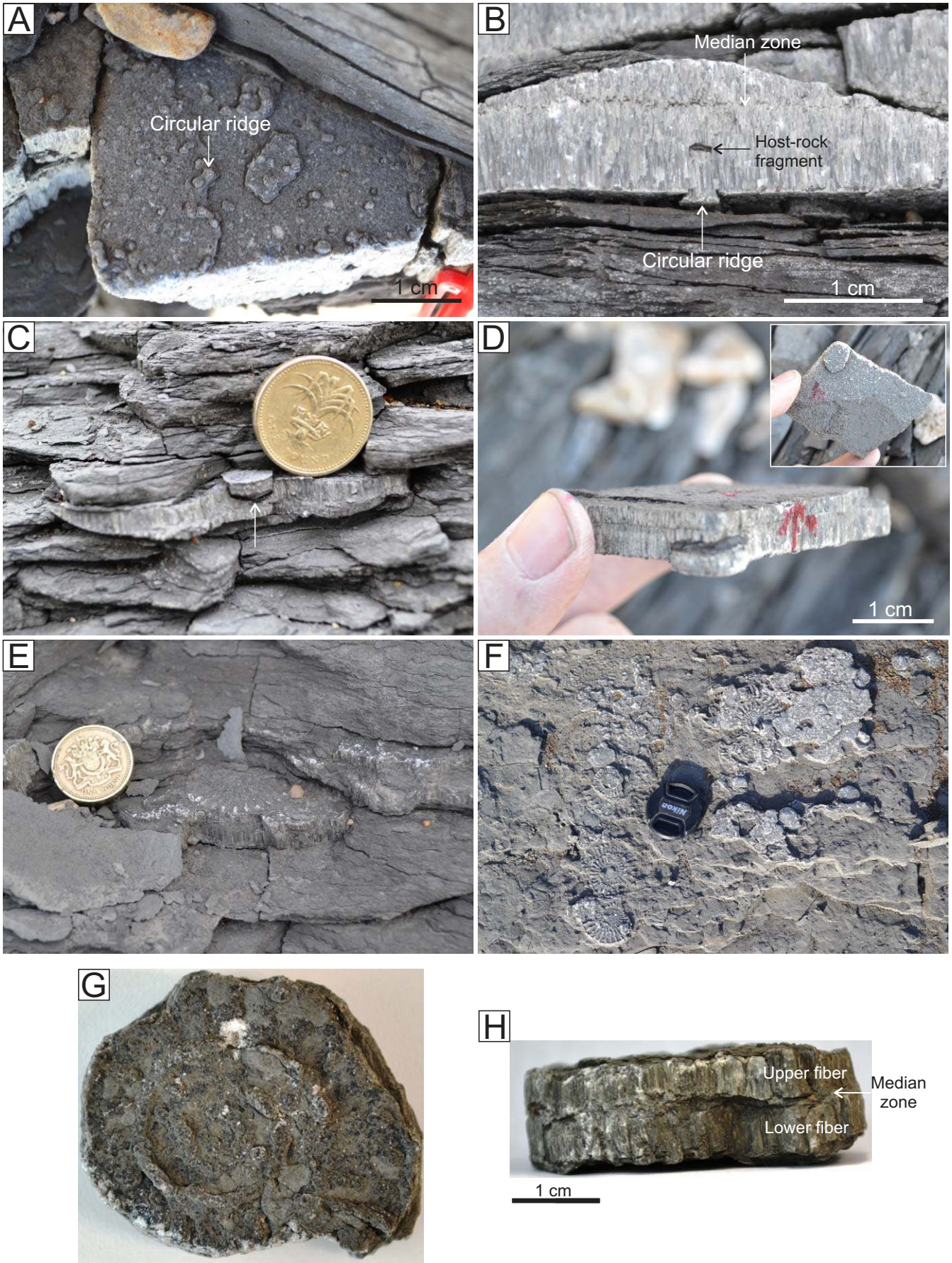
A
Circular ridge
1 cm
B
Median zone
Host-rock fragment
Circular ridge
1 cm
C
D
1 cm
E
F
G
H
Upper fiber
Median zone
Lower fiber
1 cm

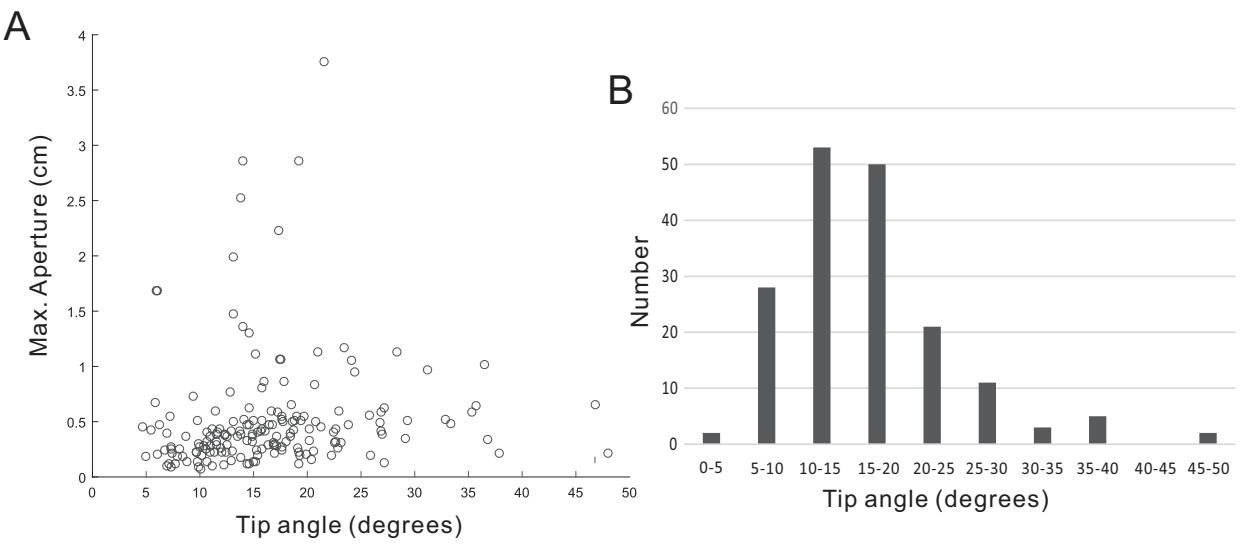
A
Max. Aperture (cm)
Tip angle (degrees)
B
Number
0-5
5-10
10-15
15-20
20-25
25-30
30-35
35-40
40-45
45-50
Tip angle (degrees)

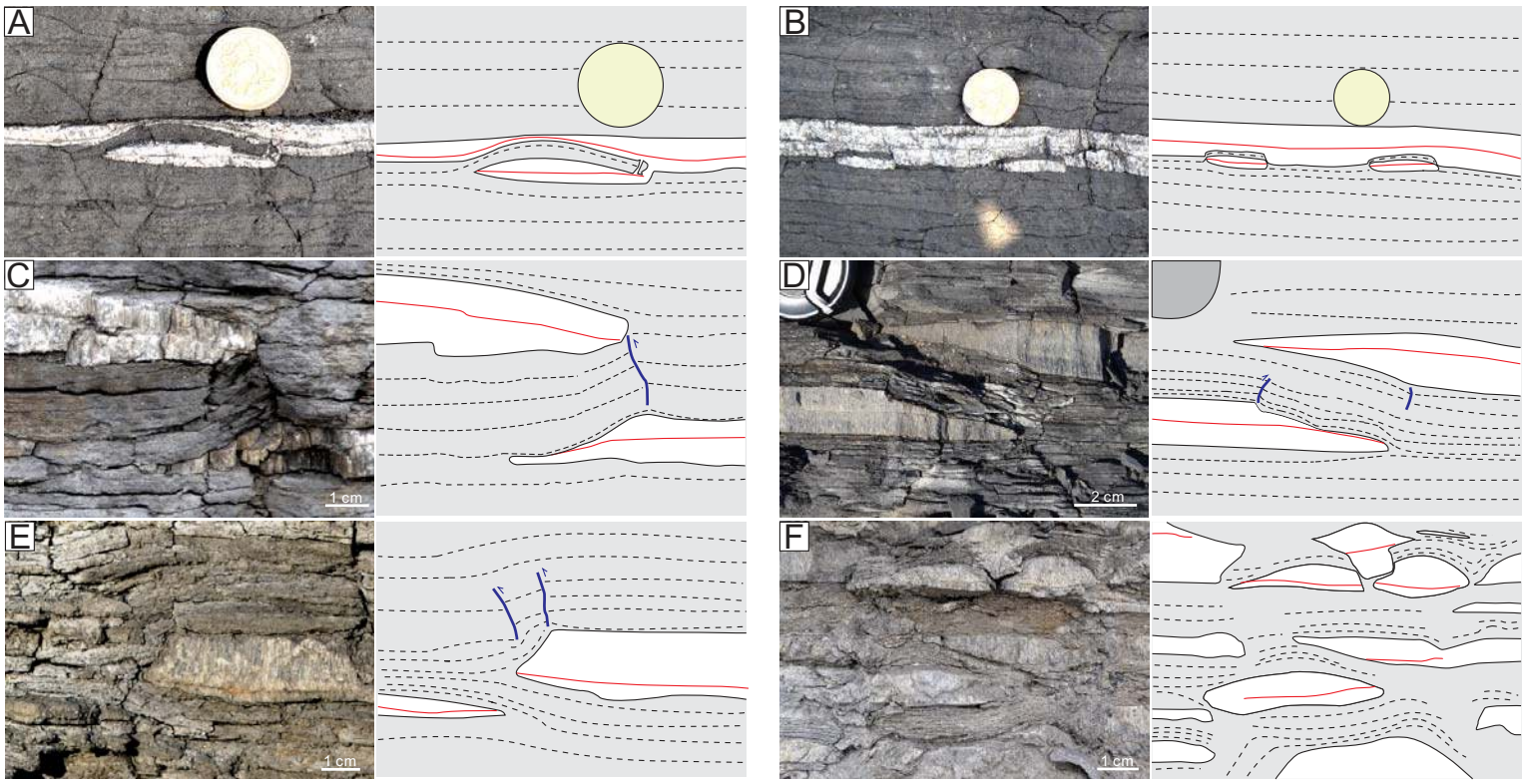
A
B
C
1 cm
D
2 cm
E
1 cm
F
1 cm

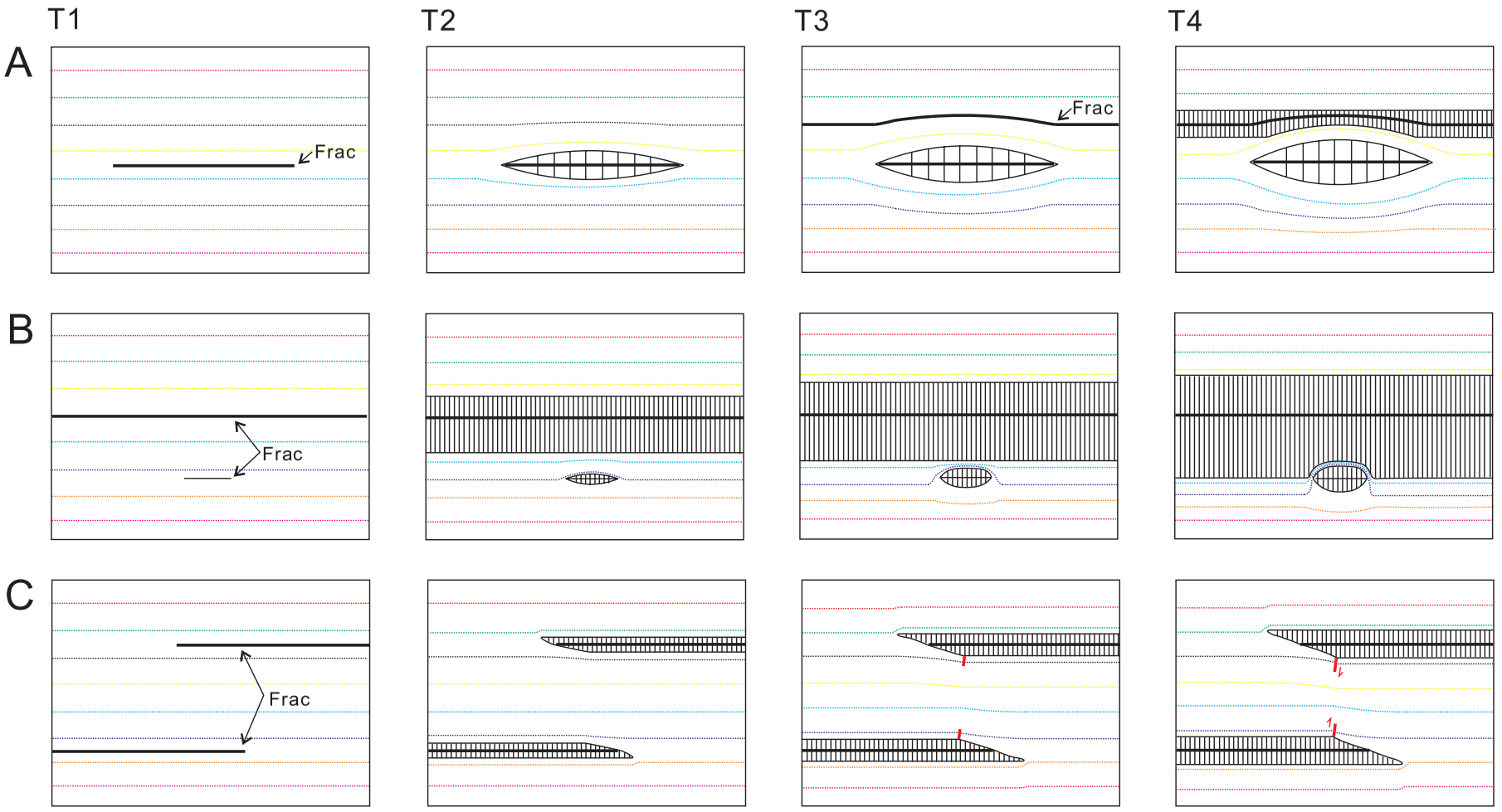
T1
T2
T3
T4
A
B
C
Frac
Frac
Frac

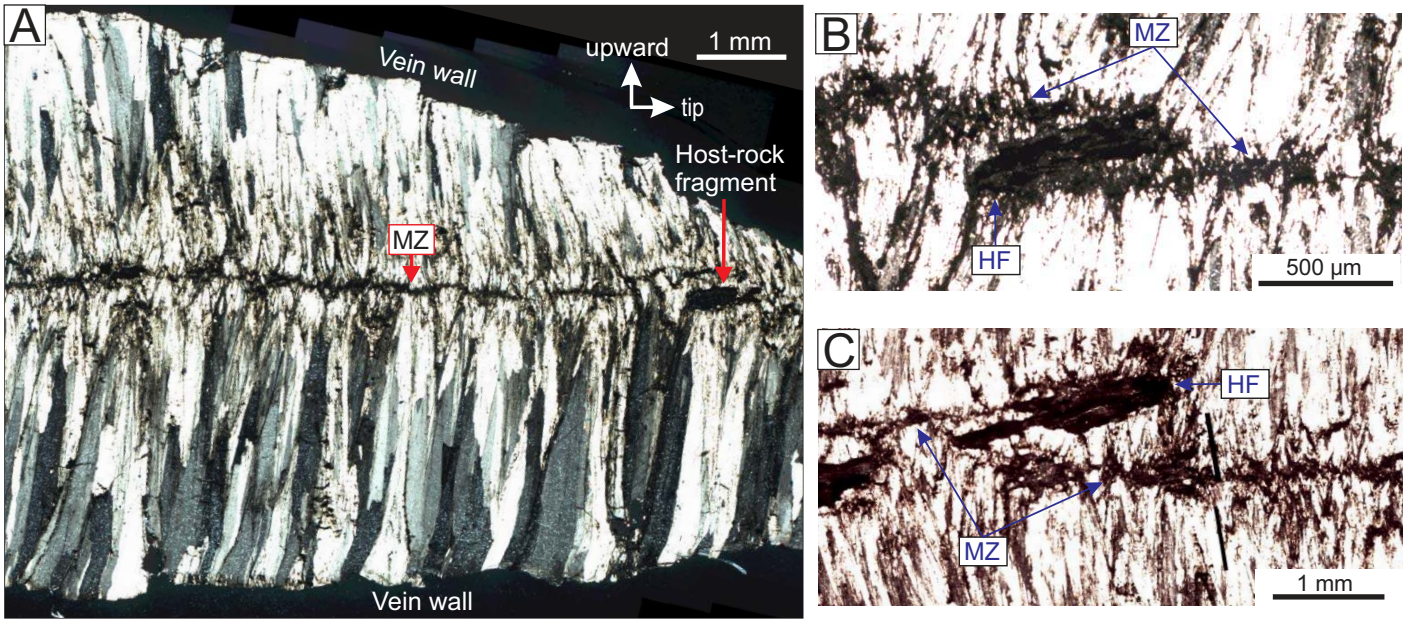
A
Vein wall
upward
1 mm
tip
Host-rock
fragment
MZ
Vein wall
B
MZ
HF
500 µm
C
HF
MZ
1 mm

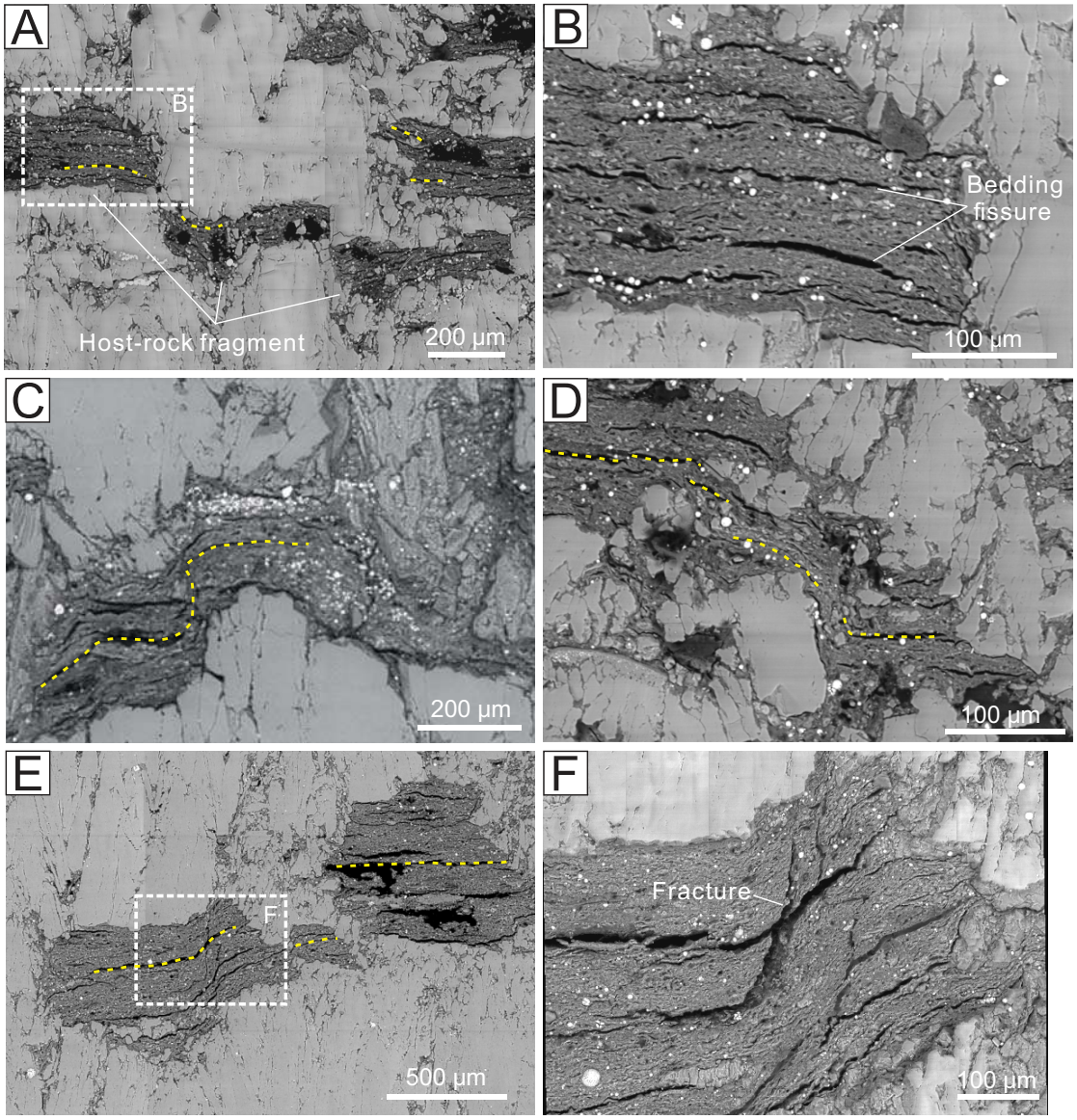
A
B
Host-rock fragment
200 µm
B
Bedding fissure
100 µm
C
200 µm
D
100 µm
E
F
500 µm
F
Fracture
100 µm

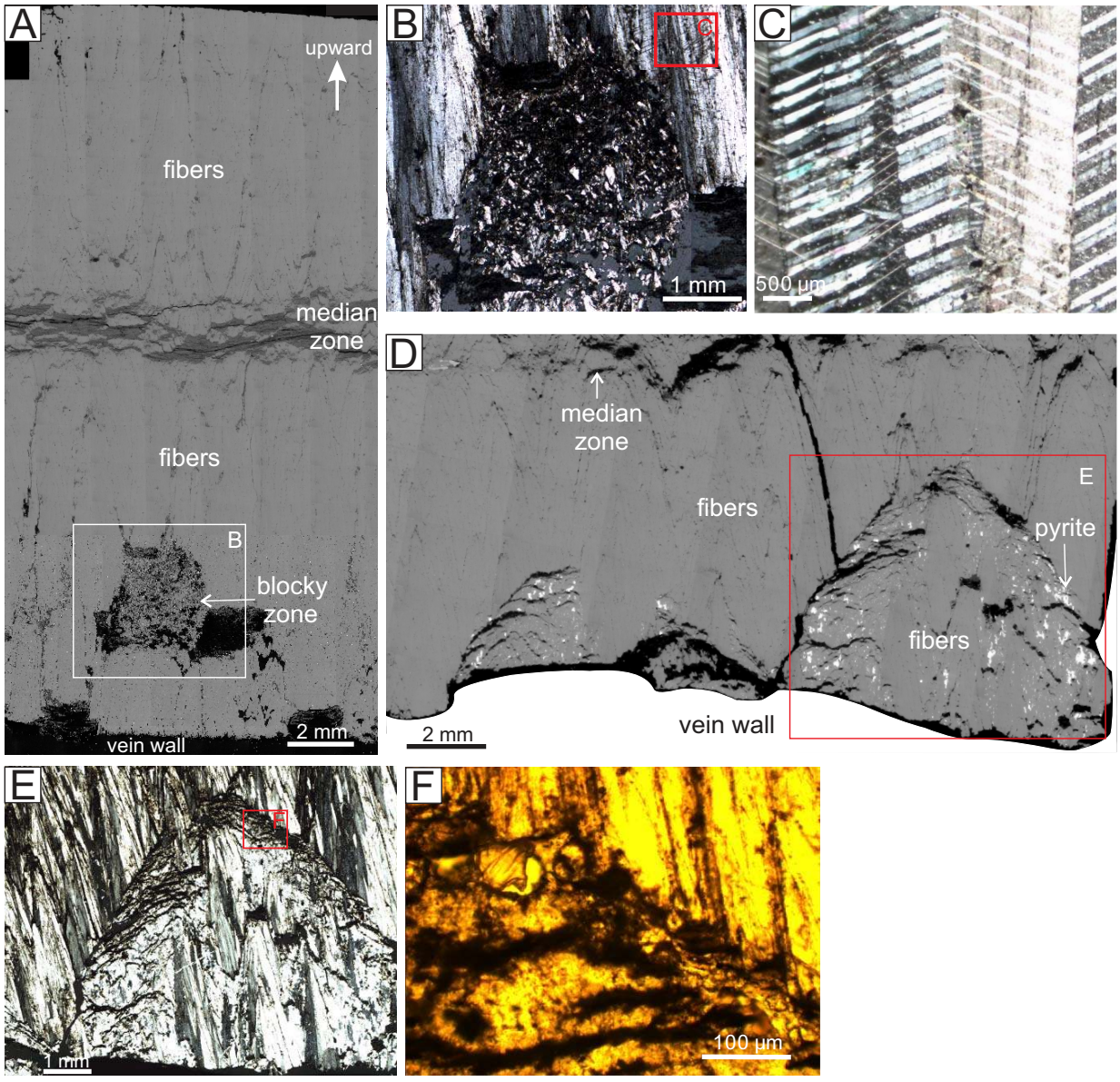
A
upward
fibers
median
zone
fibers
B
blocky
zone
vein wall
2 mm
B
1 mm
C
500 µm
D
median
zone
fibers
E
pyrite
fibers
2 mm
vein wall
E
1 mm
F
100 µm

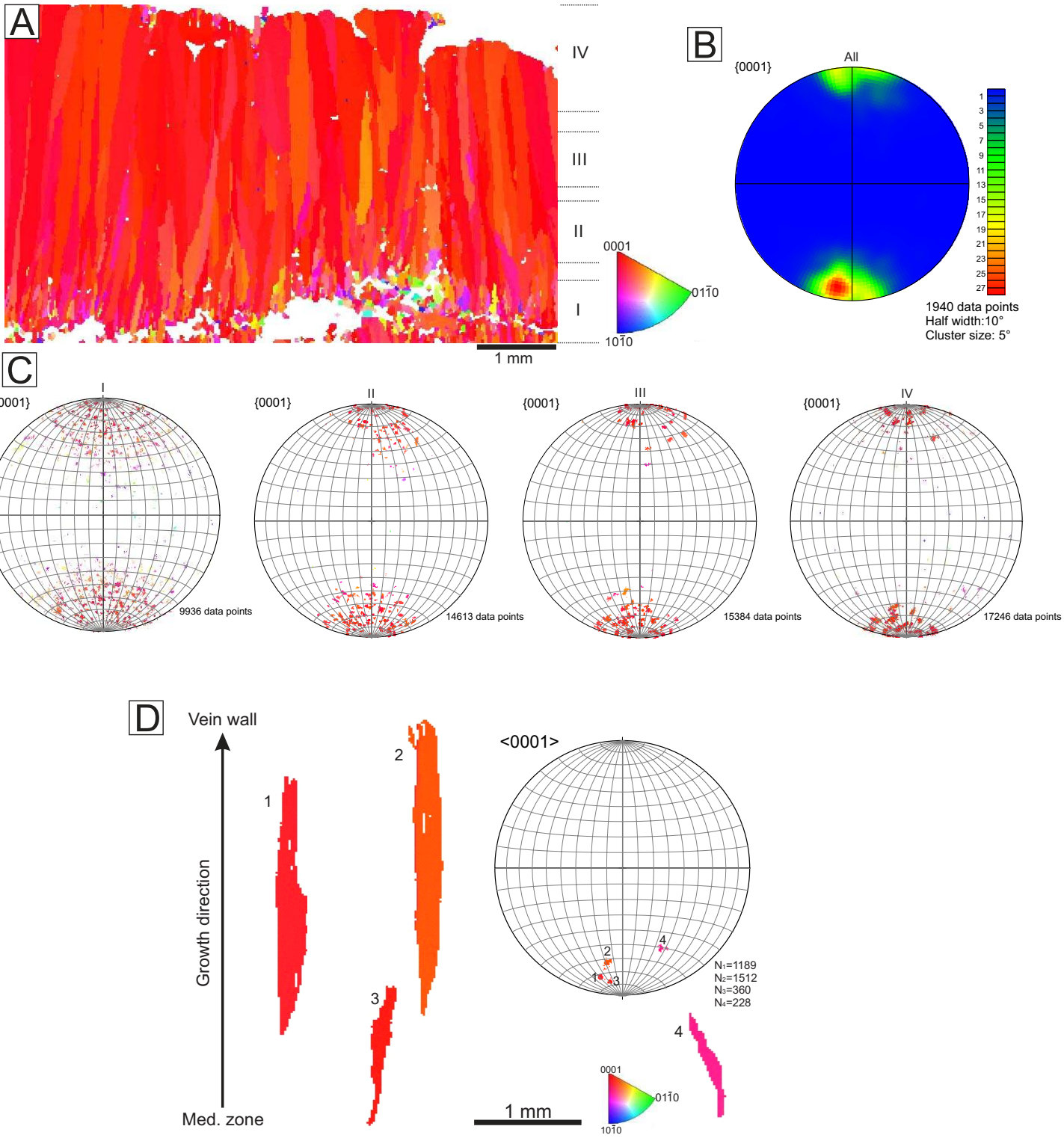
A
IV
III
II
I
0001
01$\bar{1}$0
10$\bar{1}$0
1 mm
B
{0001}
All
1
3
5
7
9
11
13
15
17
19
21
23
25
27
1940 data points
Half width:10°
Cluster size: 5°
C
I
{0001}
9936 data points
II
{0001}
14613 data points
III
{0001}
15384 data points
IV
{0001}
17246 data points
D
Vein wall
Growth direction
Med. zone
1
2
3
4
<0001>
N₁=1189
N₂=1512
N₃=360
N₄=228
0001
01$\bar{1}$0
10$\bar{1}$0
1 mm

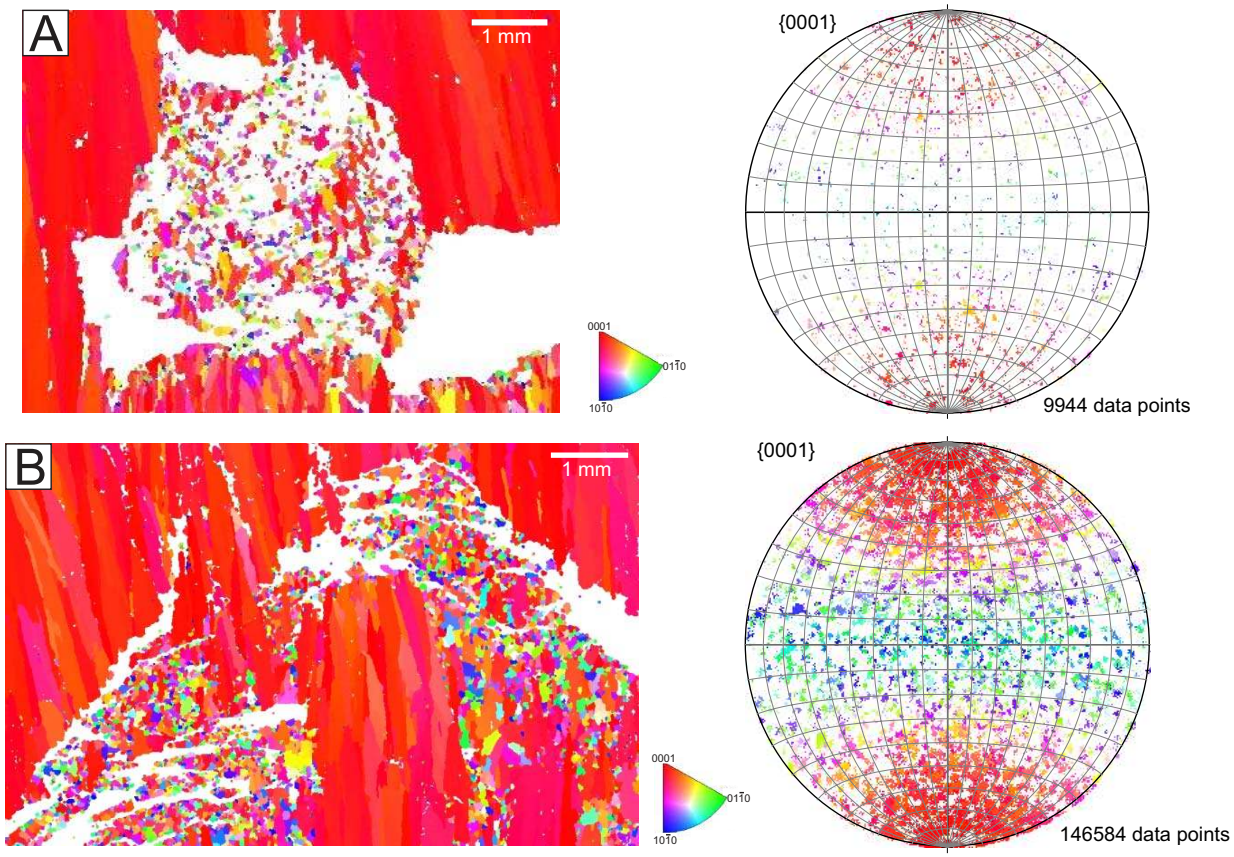
A
1 mm
0001
01$\bar{1}$0
10$\bar{1}$0
{0001}
9944 data points
B
1 mm
0001
01$\bar{1}$0
10$\bar{1}$0
{0001}
146584 data points

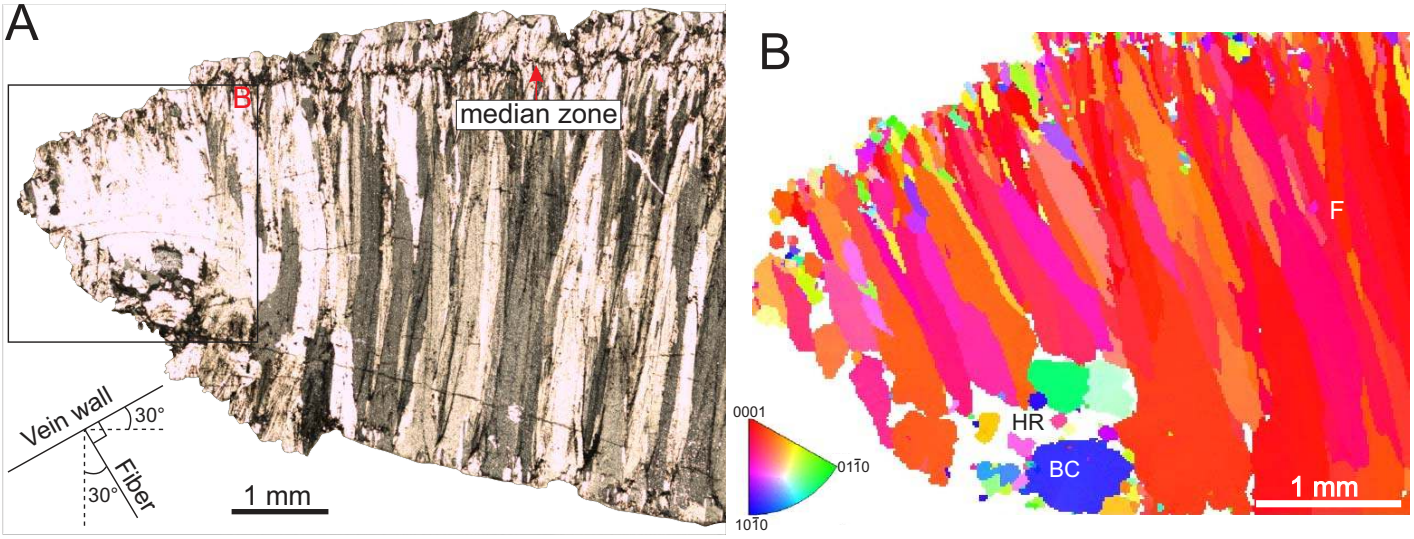
A
B
median zone
Vein wall
30°
30°
Fiber
1 mm
B
F
HR
BC
0001
01$\bar{1}$0
10$\bar{1}$0
1 mm

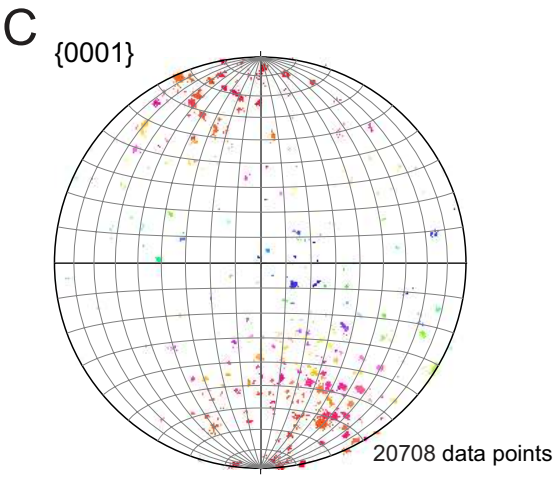
C
{0001}
20708 data points

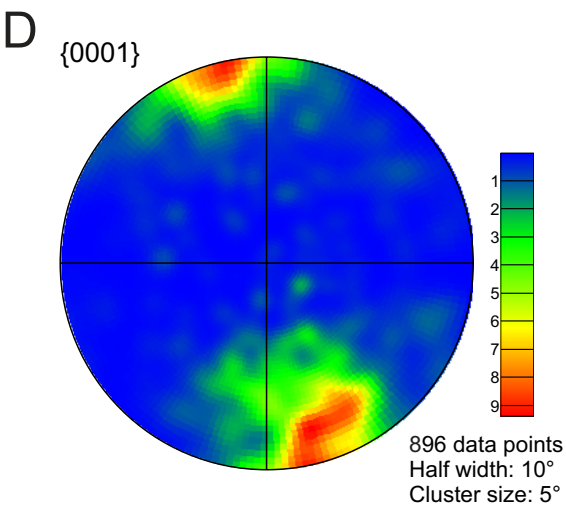
D
{0001}
1
2
3
4
5
6
7
8
9
896 data points
Half width: 10°
Cluster size: 5°

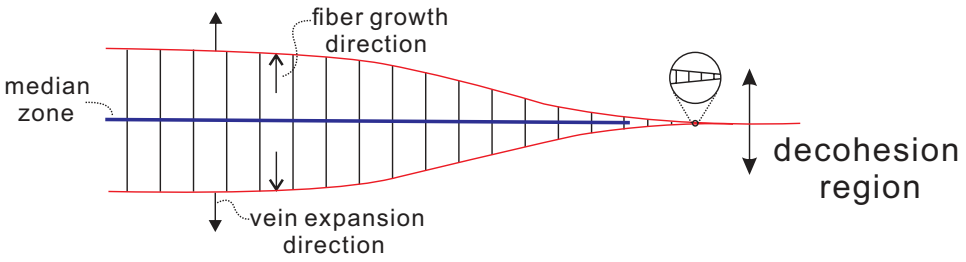
fiber growth
direction
median
zone
decohesion
region
vein expansion
direction